IN-SITU IMPREGNATION OF POLYMER MATRIX WITH COPPER POWDER DURING ADDITIVE MANUFACTURING

By

NAZMUL HAQUE

Bachelor of Science in Naval Architecture and Marine Engineering

Bangladesh University of Engineering and Technology

Dhaka, Bangladesh

2017

Submitted to the Faculty of the
Graduate College of the
Oklahoma State University
in partial fulfillment of
the requirements for
the Degree of
MASTER OF SCIENCE
July, 2020

IN-SITU IMPREGNATION OF POLYMER MATRIX WITH COPPER POWDER DURING ADDITIVE MANUFACTURING

Thesis Approved:

Dr. Hadi Noori

Thesis Adviser

Dr. Sandip P. Harimkar

Dr. Shuodao Wang

ACKNOWLEDGEMENTS

At first, I want to express my gratitude to the Almighty God for giving me the patience and helping me during this whole journey.

Also, it feels great to acknowledge the support of my advisor Dr. Hadi Noori, thanks to him for always guiding me and never let me walk alone. He has taught me to be detail-oriented and be patient while looking for a solution. It was a great privilege and honor to work under his guidance. Without his immense support, it would not have been possible to complete the research successfully.

I would also like to thank my committee member Dr. Sandip P. Harimkar, and Dr. Shuodao Wang, for always supporting me. Their door was always open for me whenever I needed any help.

The support of my family was undoubtedly the most important factor that pushed me to work hard. Thanks to my parents and their sacrifices that gave me a platform to pursue my dreams. I also wish to thank my loving sister and younger brother, who provides me unending inspiration. I would also like to acknowledge my colleagues and friends for their continuous help and supports.

Name: NAZMUL HAQUE

Date of Degree: JULY, 2020

Title of Study: IN-SITU IMPREGNATION OF POLYMER MATRIX WITH COPPER POWDER DURING ADDITIVE MANUFACTURING

Major Field: MECHANICAL AND AEROSPACE ENGINEERING

Abstract: The fillers are used to increase the functional properties of polymer matrix composites (PMCs). Additive manufacturing can be potentially used to tailor the PMCs' properties through customization of the spatial architecture of fillers (heterogeneous phases). In this study, a novel additive processing of PLA-copper composite is introduced. The fused deposition modeling (FDM) process was utilized as a platform to customize the spatial architecture of copper fillers in the 3-D structure of the PLA matrix. Prior to the extrusion process in FDM, the grooves were made on the surface of PLA filament by the knurling process. Based on the final design requirements, selected grooves were filled with copper powders. The copper powders were emulsified into liquid starch before introducing them to the groove regions. The geometry of the grooves, the interval between them, and the size/type of the powders can be independently changed to control the amount/distribution and size/type of the fillers in the final PMC product. Monolayer samples were manufactured layer by layer with a layer height and width of 0.6 and 25 mm, respectively. The PMC was devised to have a 20 mm length at the middle of samples with 90 mm length. After printing, the samples were treated with 3 kW microwave exposure for 30, 60, 75, and 90 seconds. Both treated and non-treated samples were subjected to uniaxial tensile tests to assess their fracture energy. For all samples, the fracture was brittle at the interface between the layers. The samples with PMC sections showed inferior fracture strength in comparison with pure PLA samples. This result was attributed to the presence of imperfections (voids and micro-cracks) at the interlayer areas. The microwave treatment for 75s significantly improved the fracture energy of composites. The microwave heating helped in enhancing the interlayer bond strength through the interaction with copper particles. Different mechanisms are suggested to explain this improvement. Further studies are required to assess the mechanisms.

TABLE OF CONTENTS

Chapter Page

LIST OF TABLES

Table Page

LIST OF FIGURES

Figure Page

CHAPTER I

INTRODUCTION

1.1 Overview of Polymer Matrix Composites (PMCs)

With the fast-technological advancements, the need and individual criteria for advanced materials are becoming more stringent. The research track of developing new materials seems moving away from the trend of observation and working with experiences. Currently, the trend is evolving more towards designing materials having specified properties. The development and manufacturing of composite materials are deemed promising to address the ever-changing demands for novel properties.

The composites are multi-phased systems that consist of a matrix and dispersed reinforcement/filler materials. The matrix phase can contain polymeric and non-polymeric material based on specific requirements and applications. These matrix materials play a vital role in the composites by keeping the spacing and proper orientation of the secondary phases (reinforcements/fillers). Also, they can protect the fillers from harsh environments and abrasion.

The polymer matrix composites (PMCs) involve a polymer matrix phase and secondary phases as reinforcements or fillers. In almost every area of modern life, PMCs are present-from parts in personal gadgets to a vast range of automotive components. The polymers are mainly made up of repeating carbon and hydrogen bonds that are chemically interconnected to form a chain [1]. Based on the processing methods or applications, the polymers typically used as matrix are either elastomers, thermoplastic, or thermosetting polymers. In comparison with other materials, the polymers can offer some high-end properties such as lower density, high corrosion resistivity, better thermal, and electrical insulation [2]. Furthermore, they provide easy formability and suit for economical mass production. Also, the equipment used to process PMCs is relatively cheap, and the processing techniques are mostly automated.

The reinforcements or the secondary phase in composites can work as the major element for load-bearing or other mechanical and physical properties. The interphases between the primary (matrix) and secondary phases, shown in Fig. 1, work as a transition zone for the loads. The types and volume fraction of the matrix and reinforcement are critical for the end properties of the composite. The geometry of the reinforcements/fillers and the nature of interfaces are some other important factors that play a vital role in determining the properties of PMCs [3].

Strong bonding between the polymer matrix and reinforcement/fillers is always desired for load-bearing applications. The interphases (represented by the grey color in Fig. 1) are usually formed as a result of the interaction between the reinforcements (represented by the black region) and the polymer matrix (represented by the white region). At these interphases, the properties may be the same as the bulk matrix, or they may have some different characteristics resulting from the interaction of the phases [3]. With an increase in the volume fraction of reinforcements or the decrease in their size having the same volume fraction, these interfaces become more interconnected and widespread among the particles. This eventually results in the interfaces act as the effective matrix material, making the initial bulk matrix a discontinuous phase [4].

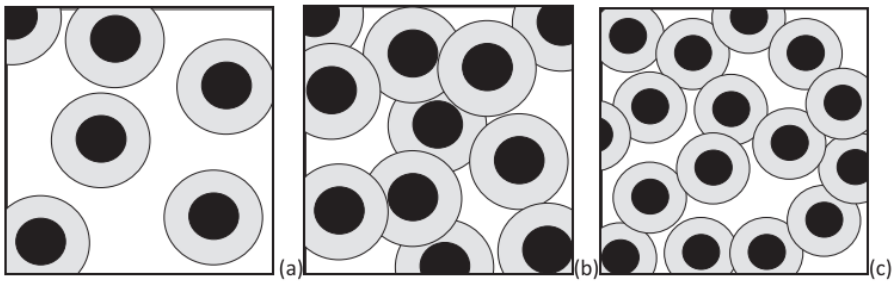

Fig. 1. (a) The interphases between matrix (in white) and secondary phase (in black) are shown in gray color. In (b) and (c), it is shown that the interconnected path develops with the increase in the volume fraction of the reinforcement. [3].

1.2 Properties of PMCs

Regarding the mechanical properties, the key advantage of the PMCs is that they offer a high specific strength compared to the constituent materials. For PMCs, the stiffness and strength are provided by the reinforcement phase. Compared to the matrix materials, generally, the reinforcing phases are stiffer, stronger, and harder. The particles or fibers are usually used as reinforcement materials. The particulates can be in the form of a regular or irregular geometrical shape, platelets, or spheres [5]. The dimensions of the particulate composites are approximately equivalent in all directions. In terms of strength, compared with the continuous fiber-reinforced composites, the particulate composites are usually less stiff and weaker [5]. In terms of processing, however, they can be processed at a relatively cheaper cost. Dependent on the involved materials, there is a threshold amount of particulate reinforcements, which makes PMC brittle and causes processing difficulties [6,7].

For fibers, the length is relatively greater compared to other dimensions. The aspect ratio, which is represented by the ratio of the largest dimension to the smallest one, varies significantly with the geometry. Usually, the aspect ratio in the case of continuous/long fibers is much higher compared to the discontinuous/short fibers, which maintain a smaller aspect ratio. Also, when it comes to the

orientation of the fibers in the matrix, the continuous fibers generally tend to maintain a preferred orientation. In contrast, a random orientation is usually seen in the case of discontinuous fibers. Some schematics of PMCs with continuous and discontinuous fibers are given in Fig. 2 [8]. Due to the differences in geometry, there are various processing methods for the composites. Usually, continuous fibers sheets are piled together to form a laminate having a preferred fiber orientation [9]. The fibers volume fraction can go as high as 60-70 volume percentages based on the desired stiffness and strength requirements [10]. As a practical matter, the smaller the fiber diameter, the higher is the processing cost [11]. The continuous fiber reinforcement causes the PMCs to have anisotropy, which is characterized as a directional property. PMCs with continuous fibers show the highest tensile strength when the mechanical loads are applied parallel to the direction of the fibers and show the lowest strength when loaded in the orthogonal direction [10]. The inherent anisotropic properties of these composites make them suitable for complex practical loading conditions.

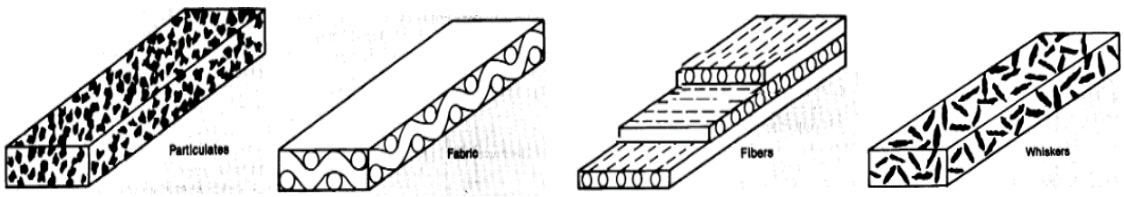

Fig. 2. Different shapes of reinforcements/fillers for PMCs [8]

The quality and properties of the end products highly depend on the nature and quality of the reinforcements. As shown in Fig. 3, the highest quality of PMCs with high strength and stiffness can be obtained by using continuous fiber. However, it increases the manufacturing cost compared to the others. Unlike the discontinuous reinforcements, the continuous fiber reinforcements offer higher flexibility in increasing the fiber volume percentages without downgrading the fracture and failure properties of the composites [12].

For the discontinuous fibers or particles, it is also possible to achieve a higher strength value by maintaining a proper filler aspect ratio and alignments. The discontinuous fibers cause more isotropy in the properties of the composites. Practically, maintaining a proper alignment within the discontinuous fibers/particles is a technical difficulty. The random orientation causes the discontinuous fiber-reinforced composites to have a lower stiffness and strength value compared with the continuous fiber-reinforced counterparts. The low cost of discontinuous fillers makes them perfect for use in the applications where the modulus or strength is less important, and the cost plays a more important role.

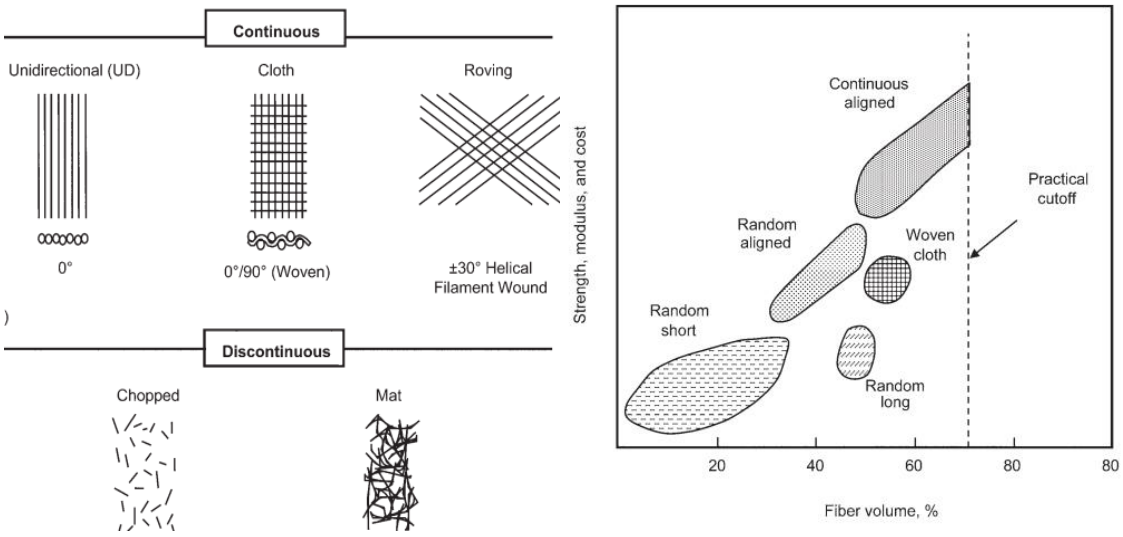

Fig.3. Fiber orientation and properties of PMCs with fiber volume percentages [12]

For particulate reinforcements, the reinforcements or fillers can be polymer particles or powders, metal particles, ceramic whiskers, etc. Dependent on the application and service conditions of the PMCs, the mechanical properties may be compromised by adding higher filler contents to achieve other specific properties such as electrical or thermal conductivity [13]. There is also a trend of developing PMCs using reinforcement particles in the nanophase. These nanophase particles are also classified differently based on their geometry. One of the classifications defines the

nanoparticles into four groups: 0-D – iso-dimensional particles, 1-D – nanotubes, 2-D – platelets, and 3-D – structures, particularly networks of nanoparticles. For any specific materials, the nanoscale phase causes the surface area of that given quantity to increase dramatically. As a result, a significantly larger number of ions/molecules/atoms becomes available to interact with the matrix on the surface.

1.3 Conventional Manufacturing Processes for PMCs

For polymer matrix composites, the manufacturing method plays a vital role in determining the end properties of the product. It is critical to understand the effect of different process parameters on the composites. Currently, there is a large number of different polymers and fillers available in the PMC industry. In processing methods for PMCs, the necessary stages typically involve i) resin-filler impregnation, ii) structure forming, iii) heat treatment for thermoplastic polymers, or curing for thermoset polymers [14]. The order of these stages is different for different processes. A list of traditional PMC manufacturing processes and their characteristics are presented in Table 1 [15].

The traditional PMC manufacturing processes are highly labor-oriented and time-consuming. Which eventually results in a higher manufacturing cost. The labor cost related to the production of composites takes up a significant part of the overall manufacturing cost for manual lay-ups [14]. Moreover, during the manufacturing process, unintentional human error causes manufacturing damages like irregularities or voids. These adversely affect the properties of the composites, making them unsuitable for service conditions. Due to these facts, the manufacturers are moving towards developing fully automated PMC manufacturing processes. The term automation refers to the computerization of a process to minimize the human-machine interaction. Automation revolutionized the manufacturing industry by increasing quality standards and production rates [15].

As the PMCs have already gained their application in many structural components due to their light weights, fast and easy processing will allow the PMCs to replace many conventional materials. Most of the current PMC manufacturing processes are not suitable for large-scale production. Processes such as hand lay-ups are suitable for small scale production of customized parts. On the other hand, the processes for large scale production, such as injection molding, are not suitable for complicated designs because of the requirement of individually customized molds. There are some automated PMC manufacturing processes currently available in the industry. Among them, filament winding (FW), resin transfer molding (RTM), laminated object manufacturing (LOM), automated fiber placement (AFP), and automated tape lay-up (ATL) are well received in the industry [16]. The high expense of advanced customized machinery and the limitations in manufacturing complex parts are restrictive factors in the use of these processes. Fig. 4 summarizes the conventional PMC manufacturing processes and illustrates a comparison of tensile properties of the fiber-reinforced PMCs considering different manufacturing techniques.

Table 1. A summary of different traditional PMC manufacturing processes [15].

Technique	Characteristics	Examples
Sheet molding	Fast, flexible, 1-2" fiber	SMC automotive body panels
Injection molding	Fast, high volume very short fibers, thermoplastics	Gears, fan blades
Resin transfer molding	Fast, complex parts, good control of fiber orientation	Automotive structural panels
Prepreg tape lay-up	Slow, laborious, reliable, expensive (speed improved by automation)	Aerospace structures
Pultrusion	Continuous, constant cross-section parts	I-beams, columns
Filament winding	Moderate speed, complex geometries, hollow parts	Aircraft fuselage, pipes, drive shafts
Thermal forming (future)	Reinforced thermoplastic matrices; fast, easy repair, joining	All of above

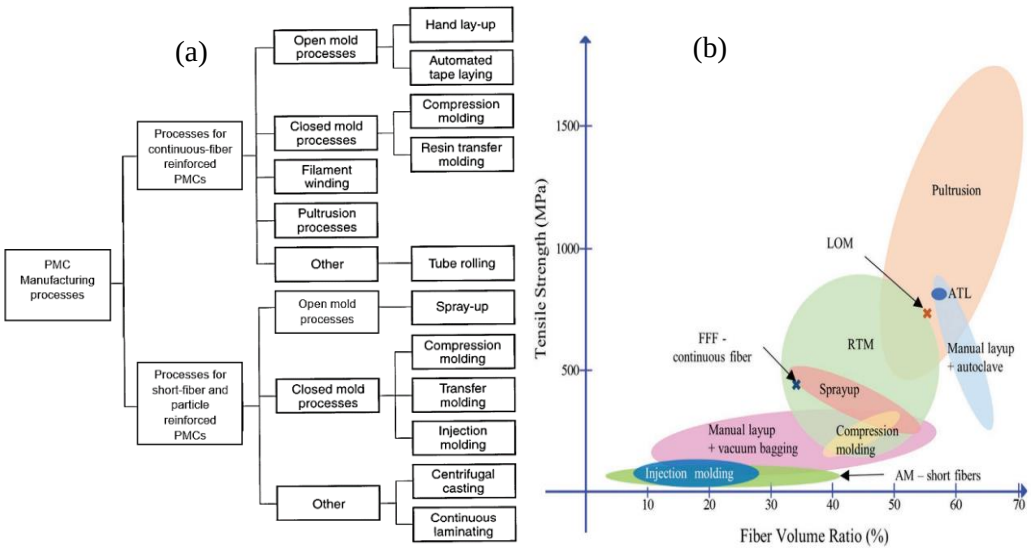

Fig. 4. (a) A tree chart of conventional PMC manufacturing processes (b) a comparison of the tensile strength of fiber-reinforced PMCs manufactured with different methods [17]

The continuous fiber PMC processes such as spray-up molding and hand lay-up methods are prolonged and inconsistent processes. These processes are highly labor-intensive and give one-sided finished output. The prepreg process is continuous, but the products have a delamination problem and relatively limited durability. The filament winding process is limited by the geometry of the product due to the need for complex numerical programs. The pultrusion process often has the die jamming problem. Also, the improper fiber wetting and fiber breakage are significant drawbacks of these processes. The use of excess resin limits the strength of the composites. The mold-based manufacturing processes (RTM, injection molding) are costly due to the need for customized molds for different parts. These processes also require mold-filling analysis, which is complex and time-consuming. The spray lay-up requires relatively longer curing time with a high waste factor. The low volume percentage of reinforcement also limits its applicability in the processing of PMCs. The automated lay-up process, which is highly used in airframe manufacturing, is limited to flat surfaces.

The manufacturing processes for short fibers and particulate reinforcement PMCs are complex in terms of controlling different process parameters such as shape and size of the fillers, their volume percentage, and orientation. In practice, the compounders like twin-screw extruders, and Banbury mixers are usually used for uniformly mixing the fillers with the polymer matrix. Although the nanofillers make a significant improvement in the properties of the PMCs, their processing is more challenging compared to the other types of PMCs. For nanofiller reinforced PMCs, a modified form of RTM called the vacuum assisted RTM (VARTM) is typically used. The VARTM is a commonly used prototyping method that uses the vacuum as a processing environment. This process gives very high surface fining, and freedom of using higher filler volume percentage at a low processing cost. However, the resins should have low viscosity [18]. The viscosity-related problems can be overcome by the autoclave method. Nevertheless, it is expensive compared to other processing techniques. Overall all the nanofiller-reinforced PMC processing requires more labor skills.

Although these processes have some of their limitations, they are considered as the benchmark for the recently developed automated additive manufacturing processes. The current additive manufacturing techniques can develop complex geometries without any requirement for customization in tooling and offer relatively less waste of materials. The fast processability of the complex designs makes the additive processing very suitable for prototyping. Moreover, due to the enormous advantages in the application and processing flexibilities of the PMCs, it is on high demand to integrate these materials with additive manufacturing processes.

1.4 Additive Manufacturing (AM) of PMCs

Additive manufacturing (AM) is a processing method by which the materials are joined or welded layer by layer in order to construct the 3D structure of the design [19]. The additive manufacturing technology is enabling the designers and manufacturers to produce more complicated products. The increasing research in this area is also helping to expand the field of application for AM from the food supply and packaging industries to biological systems, aerospace, and automotive industries.

The early history of the modern additive manufacturing process can be linked to technologies of photo sculpture and topography after the 1860s [20]. The remarkable milestone in the development of the AM process was set by Charles W. Hull in early 1983 when he successfully developed an AM system (stereolithography SLA-1) to manufacture (print) a teacup [21]. The success opened up a new world for the advancement of AM technologies. Nowadays, there are many additive manufacturing technologies available in the market based on different materials and applications. Recently, a new research trend has begun to develop bioprinting to develop custom-design organs/prosthetics.

The additive manufacturing not only is impacting the production line and supply chain but also affecting the global economy. As the AM possesses some superior advantages over the traditional subtractive and forming manufacturing processes, they are also becoming more popular among the designers and manufacturers for concept proofing. It gives the flexibility to overcome a faulty design at an early stage of manufacturing, which eventually helps to eliminate the expensive and time-consuming troubleshooting stages [22]. Also, it gives more flexibility in making customized parts and prototypes. Due to the shorter R&D period and less processing steps, the key players in the manufacturing field from automobile, aerospace, medical and energy industries are rallying behind the AM processing. In 2015 alone, the revenue of AM processes was more than USD 5

billion worldwide [23]. The studies have shown that a majority of this revenue came from the polymer-based application and sales of related materials [23]. The demand for AM is shifting from developing prototypes to functional parts with the advancement in technologies and materials. Still, AM is more preferred for small scale production and making complex geometries rather than mass production of simple geometrical parts due to low-speed processing of available techniques.

1.4.1 Working Principle and Existing AM Processes

The AM process utilizes two major sequential steps, from designing the virtual CAD file to the final manufactured part. In the first step, a CAD model that contains the numerical information of the layers will be developed. In the second step, the CAD model will be utilized by the firmware of the AM machinery for constructing the physical layers of the 3D structure [24, 25]. Fig. 5 shows a flow of the steps for the AM technique.

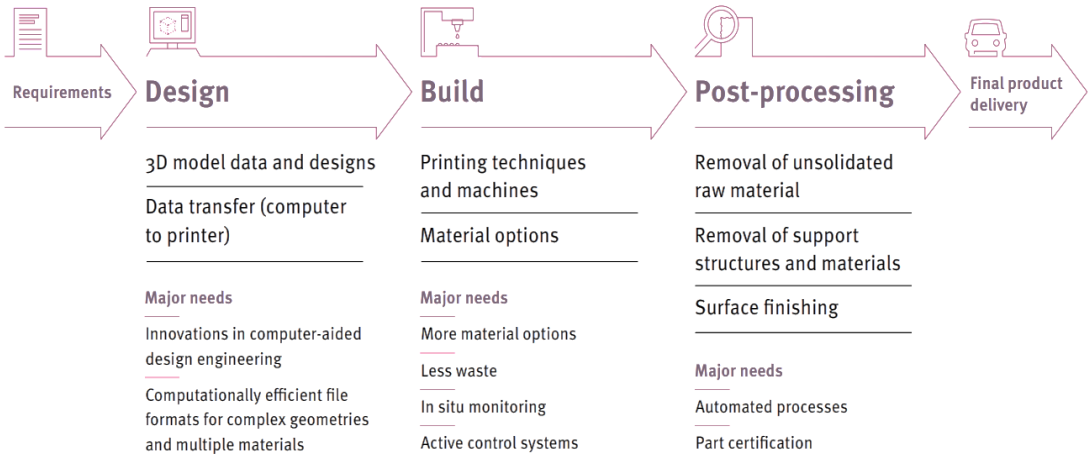

Fig. 5. An illustration of the general processing steps of additive manufacturing techniques [25].

The beginning of the design phase for any AM part starts with a software model that completely describes the geometry of the part. Any computer-aided design software can be utilized for this purpose of solid 3D modeling. Some reverse engineering tools and 3D scanning systems can also

be used to generate the CAD model. The CAD file needs to be saved in some specific file format in order to be recognized by the AM printer. This also allows the required slicing process of the CAD model to be processed by the AM machinery firmware. One of the de facto file formats to save the CAD model for AM printers is the stereolithography (STL) format [26]. In order to print the modeled part, the STL file may need some modifications, such as resizing, repositioning the virtual model on the build plate, and revising the build orientation. Before starting the print, it is necessary to set up the process parameters properly. The printer uses the numerical data of the CAD design developed by the slicer to process the materials for layer-by-layer manufacturing. Some of the designs may require support materials to compensate for overhanging features in the design. After the printing process is done, the support features need to be removed. Depending on the application, the manufactured parts may require some post-processing steps for the properties improvement before being used in their service conditions.

Though the fundamental principles are the same, it is important to classify the methods based on their differences. One way to classify the additive manufacturing systems is to consider the state of starting materials used for manufacturing. According to current technologies, we can classify the AM system into (i) solid (ii) liquid and (iii) powder-based systems [27]. Based on the materials property, deposition method, and nature of bonding of the materials, the processes can be subcategorized into seven AM processes. The schematic in Fig. 6 shows the classification of the AM processes.

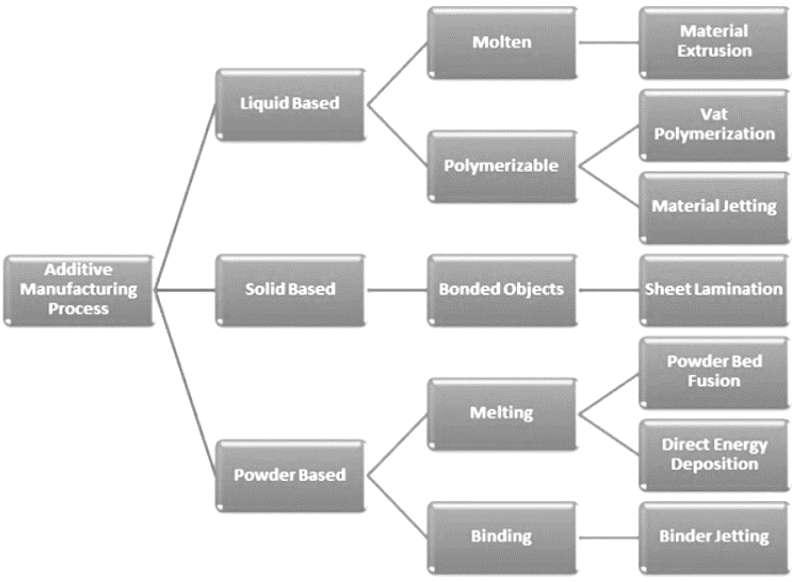

Fig. 6. Classification of AM processes [27]

The AM processes utilize a variety of different types of materials (polymers, ceramics, and metallic compositions). Also, new researches are bringing in more advanced, hybrid composites and functionally graded materials. There is an increasing demand to develop and utilize polymer composites in additive manufacturing platform. The introduction of another phase or material into the polymer matrix will add to the application of AM in the processing of novel and high-performance materials and designs.

Commercially available 3D printers can process thermosetting polymers such as epoxy, and thermoplastics such as polycarbonate (PC), polylactic acid (PLA), and acrylonitrile butadiene styrene (ABS). The epoxy resins show lower viscosity, so they need to be cured through thermally or UV-assisted polymerization [28]. As the components printed with pure polymers show low strength or other deficiencies in properties that limit the functionality of the design, they are mainly used in prototyping instead of fully functional parts.

Similar to the conventionally manufactured polymer composite parts, printed PMCs can show higher functionality than the individual constituents. In contrast, more control precision in additive manufacturing can be considered as an advantage over traditional injection molding or casting processes [29]. The development of advanced PMCs compatible with different AM printers has gained attention in academia and industry. Different AM techniques can be employed for printing PMC parts, and each of these techniques has its own limitations and advantages. A summary of different AM processes for PMCs is presented in Table 2, highlighting their mechanism, drawbacks, and advantages [30].

Table2. Different additive manufacturing processes for PMCs and their working principles [30]

Technique	State of starting materials	Typical polymer materials	Working principle	Resolution (Z direction,μm)	Advantages	Disadvantages
FDM	Filament	Thermoplastics, such as PC, ABS, PLA, and nylon	Extrusion and deposition	50–200 (Rapide Lite 500)	Low cost, good strength, multi-material capability	Anisotropy, nozzle clogging
SLA	Liquid photo-polymer	Photocurable resin (epoxy or acrylate based resin)	Laser scanning and UV induced curing	10 (DWSLAB XFAB)	High printing resolution	Material limitation, cytotoxicity, high cost
SLS	Powder	PCL and polyamide powder	Laser scanning and heat induced sintering	80 (Spo230 HS)	Good strength, easy removal of support powder	High cost, powdery surface
3DP	Powder	Any materials can be supplied as powder, binder needed	Drop-on-demand binder printing	100–250 (Plan B, Ytec3D)	Low cost, multi-material capability, easy removal of support powder	Clogging of binder jet, binder contamination
3D plotting	Liquid or paste	PCL, PLA, hydrogel	Pressurized syringe extrusion, and heat or UV-assisted curing	5-200 (Fab@home)	High printing resolution, soft materials capability	Low mechanical strength, slow

1.4.2 Additive Manufacturing of Fiber-Reinforced PMCs

A very high-quality PMC with enhanced properties can be achieved by introducing fiber reinforcements with polymers. Recent advancements in AM have developed techniques to introduce these fillers with a polymer matrix to improve their functional properties. The two most popular AM processes that are employed to fabricate fiber reinforced PMCs are direct writing and the fused deposition modeling (FDM) processes.

1.4.2.1 Continuous Fiber-Reinforced PMCs

The continuous fibers provide more strength and improve the properties better than the other types of reinforcements. Over the past few years, several studies were conducted to make the AM of continuous fiber-reinforced PMCs feasible. In one of the studies [31], the researchers used a commercially available MarkOne 3D (Markforged, USA) printer with a dual extrusion head. In one extruder, they used nylon and continuous carbon fiber in the other one. They printed a sandwich structure with continuous fiber in the middle between the nylon layers. They studied the process parameters to improve the bonding and mechanical properties of the composite [31]. Tial et al. [32] and Matsuzaki et al. [33] worked on developing novel techniques to print long fiber-reinforced composite structures. The process proposed by Tian et al. [32] is shown in Fig. 7 (a). In their method, the long fibers were introduced inside the extruder along with the polymer filament. The high temperature inside the extruder block caused the polymer filament to melt and combine with the long fibers forming a composite before coming out of the nozzle. They studied the interface properties of the layers and found a strong interface bond between the polymers and fibers. Matsuzaki et al. [33] proposed a similar methodology with some modification in the long fibers feeding mechanism. The processing method proposed by them is shown in Fig. 7 (b). Instead of directly feeding the fiber materials, they preheated them just before feeding. Due to this preheating step, a stronger bond between the fiber and polymer materials was achieved. Also, it eliminated the possibility of clogging inside the nozzle due to insufficient heating of the fibers, and the printed tensile samples showed results very similar to those processed by conventional methods. These studies opened up opportunities to print complex load-bearing structures using direct FDM printing. Namiki et al. [34] also attempted a similar experimental procedure to print continuous carbon fiber/PLA composite. Zhong et al. [35] and Nakagawa et al. [36] used FDM to print carbon fiber reinforced polymer composite parts. In these studies, they concluded that additional heat

treatment of the printed part helps in improving the bonding between the fiber and polymers. Also, surface processing of the carbon fibers increased the tensile strength by around 18%.

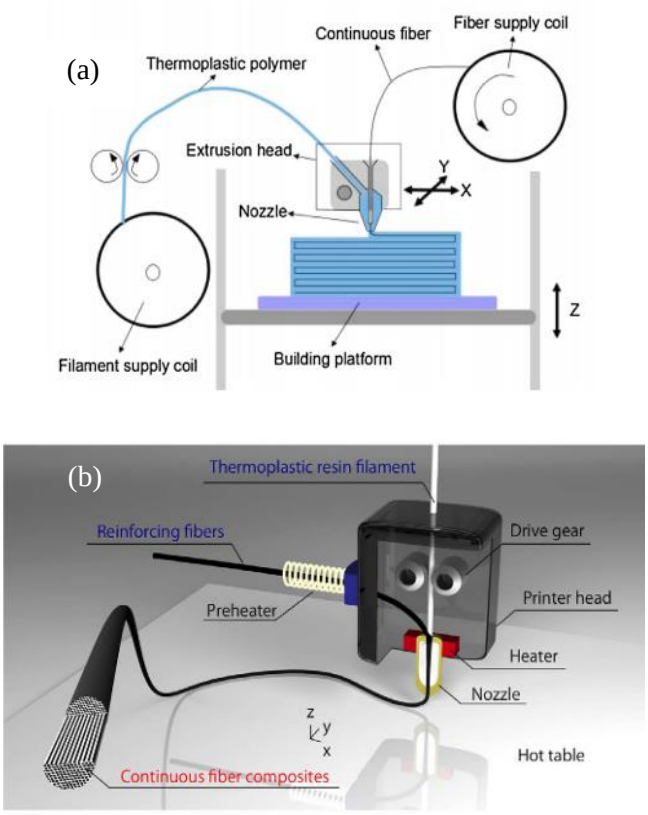

Fig. 7. Schematics of two similar AM processes for continuous fiber-reinforced PMCs as shown in (a) [32], and (b) [33]

1.4.2.2 Short Fiber-Reinforced PMCs

The polymers are mixed and blended with the short fiber reinforcements and extruded into a rod-shaped filament. These filaments are then used to print the desired geometries using commercially available FDM printers. In direct-write printing, the polymers and short fiber fillers are conventionally mixed, and the mixture is printed to form desired geometry. Because of technical difficulties such as nozzle clogging and temperature controlling, the high-volume percentage of

short fibers cannot be practically used for PMC additive manufacturing. Moreover, in the case of short fiber, it becomes difficult to achieve a smooth print surface and desired even layers [37].

As shown in different studies, additively manufactured PMCs showed high thermal, mechanical, and electrical properties by using short fibers or the discontinuous fiber reinforcements such as glass fibers, aramid fibers, and carbon fibers [38-46]. The use of short glass fibers significantly reduced the swelling effect at the nozzle and increased the rigidity of the composite [38]. Carneiro et al. [39] investigated the tensile properties of polypropylene/short glass fiber composites printed with the FDM process. For this study, they optimized different print parameters, including infill degree, layer thickness, and print direction. They obtained the highest tensile strength with 100% infill density and 0^{o} print direction with respect to the tensile direction.

Tekinalp et al. [40] investigated the effect of fiber arrangement and porosity on FDM printed composite parts. Due to the weak adhesion between the short carbon fibers and the ABS matrix, a significant increase in the formation of voids was observed. In comparison with the compression molded parts, the strength of the additively manufactured samples was lower due to the higher volume fraction of voids in the PMC structure. The presence of the short fibers reduced the interlayer porosity while the inner-bead porosity was increased significantly. The increase in fiber contents contributes to improved packing of the deposited beads resulting in smaller inter-bead voids. However, during the printing, this increased number of fiber ends results in more inner-bead voids. This phenomenon has been illustrated in Fig. 8. In their studies, they claimed that the effect of voids on tensile strength could be overcome by the proper fiber orientation in the FDM printed part.

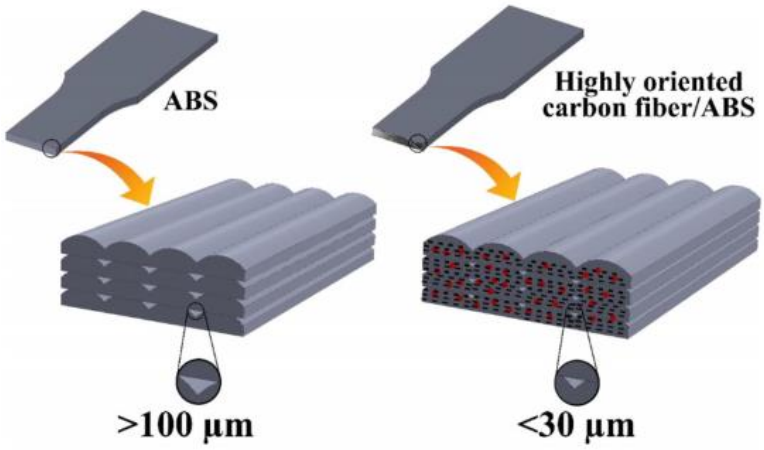

Fig. 8. Comparison of interlayer and inner bead porosity in FDM printed short fiber-reinforced composites [40].

The formation of voids remains a major problem in additively manufactured parts because it reduces the tensile strength of the composites. Recently, some studies showed that the addition of expandable microspheres could help in reducing this effect. Wang et al. [41] showed that the vapor growth carbon fibers (VGCFs) help in reducing the porosity volume fraction from 17% to 7%. These carbon fibers typically have high crystallinity with high thermal and electrical properties. The VGFCs and multiwalled carbon nanotubes (MWCNTs) are of interest as reinforcement fillers due to their high thermo-mechanical properties. Some experimental results showed that the use of VGCFs or MWCNTs with the ABS matrix increases the tensile strength of about 93% comparing with pure ABS [42]. When the porosity is required in designing moisture-actuated composites, one study showed that the water absorption capacity and relative permeability of an FDM-printed wood fiber-reinforced composite increased by around 40% [43].

The fiber content also plays a critical role in determining the properties of the composite. A study conducted by Ning et al. [44] used composite filament (FilaBot Co., Montpelier, USA) having ABS as the matrix and 5wt% of chopped carbon fiber as fillers for FDM processing. The study indicated that the strength increased up to a certain volume percentage of the fiber contents over which the

addition of fibers significantly reduced the strength of the composites. Also, high carbon fiber contents caused nozzle clogging resulting in disruption of the printing process. Some recent studies showed the voids or nozzle clogging problems could be reduced through the laser sintering process. One study showed around 22% increase in storage modulus in the selective laser sintering (SLS) printed polyamide-12/carbon nanofibre composite parts compared with pure polymeric parts [46].

The print direction also affects the composite properties. Compton et al. [45] used the direct writing process to study the effect of print direction. They prepared samples by printing in the same direction as the fibers were oriented. Fig. 9 (b) illustrates the filler orientation in the print direction and its effect on mechanical properties. Due to the alignment of the fibers, they obtained composites having a high toughness value.

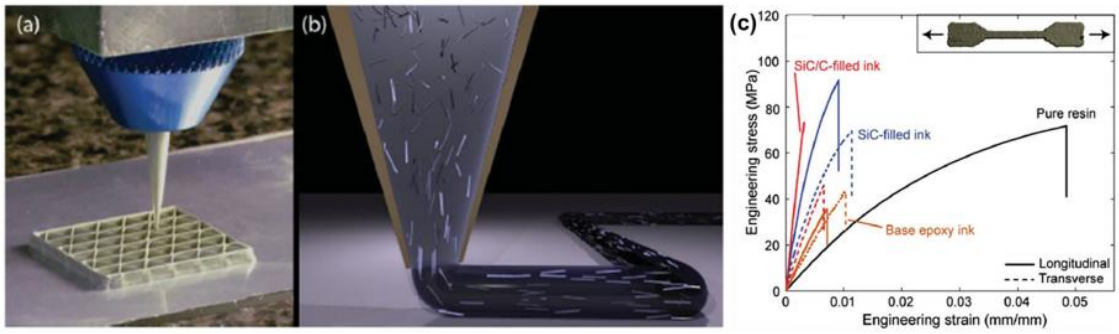

Fig. 9. (a) Direct write printing of a triangular honeycomb composite. (b) Schematic illustration of filler alignment within the nozzle during composite ink deposition. (c) Stress-strain curves for 3D printed samples with different compositions and samples cast from pure epoxy resin. [45]

1.4.3 Additive Manufacturing of Particulate-Reinforced PMCs

The addition of particle fillers can increase the functional properties of the printed composites. Dependent on the shape and properties of secondary phases in PMCs, different processing techniques can be utilized. Some studies showed that the addition of iron and copper particles

increases the tensile strength of the composites [51]. Also, the addition of glass beads with the ABS matrix showed an increase in the storage modulus of the printed composites [47]. Boparai et al. [48] showed that the addition of aluminum and aluminum oxide (Al2O3) into the nylon matrix reduces surface wear and roughness, and they increase the dielectric permittivity of the printed composites when added with UV-cured epoxies. Their study also showed a significant improvement in surface friction. Shemelya et al. [49] used the FDM printing process to print micro-size (12 microns) tungsten particle-reinforced polycarbonate composites to analyze electromagnetic and X-ray shielding characterization for space-based applications.

Ayrilmis et al. [50] used PLA with wood flour powders and extruded them together prior to AM to prepare a composite filament. They showed that the reduction in the layer height significantly reduces the formation of interlayer voids. Their study also showed that the rate of water absorption by the composite part increases significantly with the layer height because of the higher volume fraction of void contents. Hwang et al. [51] analyzed the thermo-mechanical properties of the ABS matrix composites with iron and copper particles of different sizes. Using different filler concentrations (up to 80 volume%), they prepared the samples using an FDM printing machine. They observed the effect of extrusion temperature on the viscosity and tensile strength of the printed parts. They showed that the increasing particle concentration caused a decrease in the ductility of the printed parts. A recent study by Castles et al. [52] showed an increase in the relative dielectric permittivity of (BaTiO3)/ABS composites compared with the pure ABS. They utilized the FDM process to print structures in the shape of photonic diamond crystals.

One major problem faced during AM of pure polymers is the inadequate bonding between layers and distortion due to their high thermal expansion. A study by Chung et al. [53] showed that the introduction of metallic fillers lowers the thermal expansion and keeps the layers of the composite intact, resulting in less distortion. In this study, low thermal expansion was observed in the composites having iron and copper particles in the ABS matrix [53].

In AM processes, the anisotropy in the properties is a major concern. One study showed a reduction in the anisotropic properties when ABS was combined with thermoplastic elastomers [54]. A more innovative way to control the anisotropy was demonstrated by Kokkinis et al. [55]. They used a customized printing bed having magnetic support to control the orientation of the magnetized filler particles in the polymer matrix. This technique could also be integrated with the digital light processing (DLP) to control the orientation of the magnetic fillers. Also, in SLA printing, where UV-sensitive resins are used, the magnetic field can help in the filler alignment [56].

Acrylate resins are a special form of polymers derived from methacrylic acid or acrylic acid. In liquid 3D printing, they are used as polymer matrix because of their quick recovery and drying properties. Kalsoom et al. [57] studied the thermal properties of the SLA-printed composites for heat sinking applications. They used acrylate resins as polymer matrix and reinforced it with spherical micro-diamond particles. The results showed that the heat transfer rate in the composite was improved significantly. Fig. 10 shows the comparison between the temperature profile of the heat sinks prepared with pure acrylate resin and composite mixture. Kurimoto et al. [58] also used SLA processing to prepare UV-cured resin/Al_2O_3 composite samples. They obtained an increased dielectric permittivity in the printed composite parts.

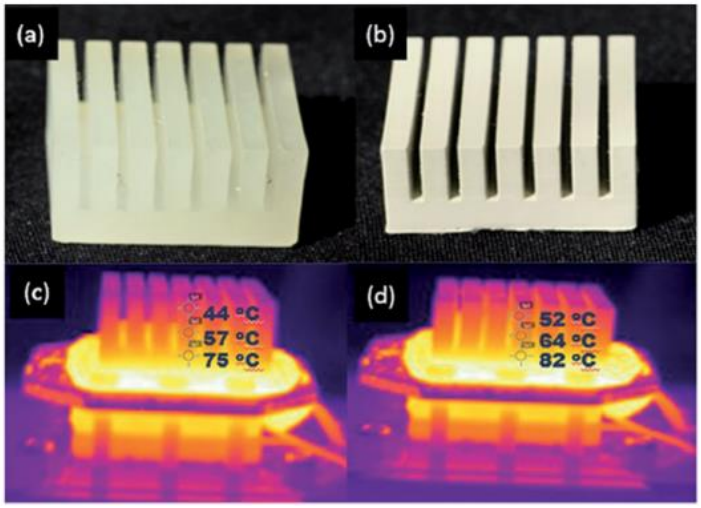

Fig 10. (a) Heat sinks prepared with the SLA technique; (b) heat sink with pure polymer resins; (c) composite heat sink with 30% (w/v) of diamond nanoparticles; and (d) temperature profile when heated to 100°C for 10 min [57]

1.4.4 Development of Screw-Based Direct Extrusion Process for PMCs

A combined extrusion-AM process has been recently proposed for the additive manufacturing of PMCs. This process will potentially eliminate the requirement of preprocessing of composite material before additive manufacturing. In this context, two very similar processes were proposed by Boyle et al. [59] and Basher et al. [60]. Both of the processes allow FDM to manufacture composite structures without using a pre-developed composite filament. Boyle et al. [59] used a commercially available Rich Rap extruder (RichRap3D, USA), and Basher et al. [60] used a commercially available Makerbot extruder (MakerBot Industries, USA), as shown in Figure. 11 (a) and (b), respectively. The extruder section was modified by adding an extra part that works as a pellet mixer. Here, instead of using the polymer in a direct filament form, both polymer matrix and different reinforcement particles are put together inside a funnel. The stepper gear mechanism mixes them and introduces the contents inside a high-temperature extruder block. The polymer melts and mixes with the reinforcement particles. Finally, the mixed composite enters the hot end

nozzle for the deposition stage. According to their obtained results, this screw-based extrusion model has shown promising aspects for industrial applications. Yet, the vibration and associated print defects are some significant drawbacks.

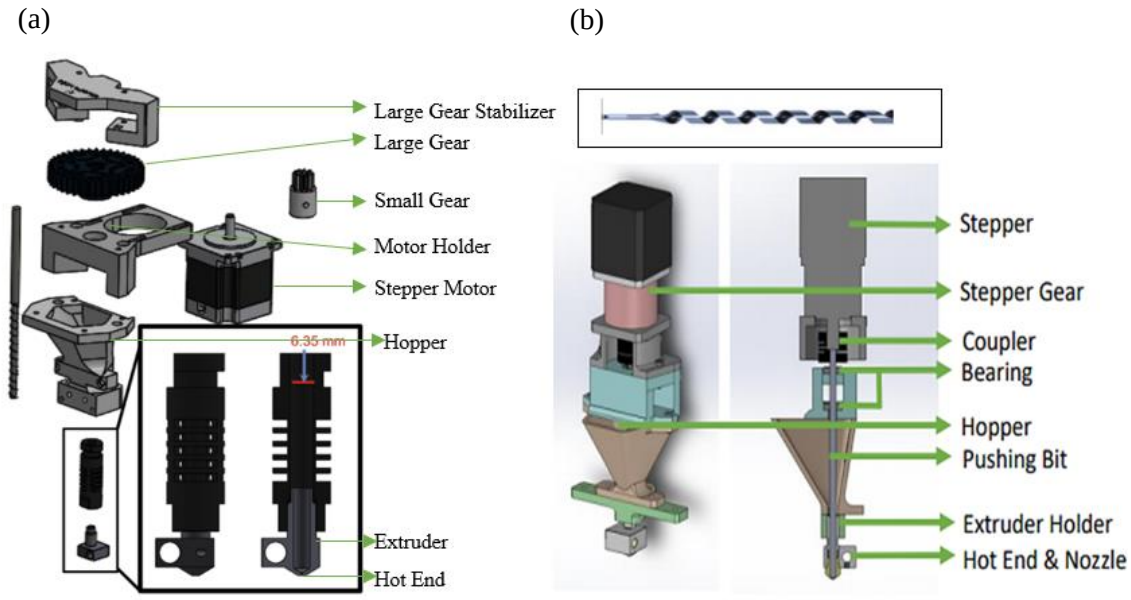

Fig. 11. (a) [59] and (b) [60] are the schematics of the screw-based 3D printing system with their major system components for direct fabrication of particle reinforced PMCs, as illustrated.

CHAPTER II

EXPREIMENTAL PROCEDURE

As reviewed in Chapter 1, the conventional additive manufacturing of PMCs, there are two sequential steps in processing. In the first step, the devised type and amount of reinforcements/fillers are mixed uniformly with the polymer matrix. Three different methods have been developed for the second step. In one method, the composite mixture is extruded in the shape of filaments with a prespecified diameter suitable for the FDM process. In one other method, the mixture will be fed into the direct writing or direct extrusion process for additive processing.

For all of these processes, the major limitation is their inflexibility for customization of the composite structure in terms of type and amount of fillers during additive manufacturing. The motivation behind the current research work lies in developing a simple and continuous PMC manufacturing process that will allow more freedom in implementing heterogeneity in the composite structure. The proposed manufacturing model will allow the introduction of different particulate reinforcement for different regions within a structure according to design and application requirements. Overall, the motivation of this work is to allow more degree of freedom in customization through a minimized processing step and time.

The objective of this study is to propose a novel technique for PMCs additive manufacturing that is capable of in-situ customization of the amount and type of fillers inside of 3D printed structure. The FDM process was selected as a processing platform for this objective.

As a brief overview of the proposed technique, the filament was knurled at devised locations. The knurled grooves served as carriers for fillers (copper powders) that were introduced into them via the impregnation step immediately before the printing process. The impregnated filaments were pushed into the extrusion nozzle for deposition on the substrate for additive manufacturing. This chapter presents the detail of the process. Also, test samples were prepared by the proposed technique. The uniaxial tensile tests were conducted to assess the fracture properties of the developed composite structures.

2.1 Materials Selection

In this study, PLA filament with a density of 1.24 g/cm^3 and a diameter of 1.75 mm was used as a matrix for the manufacturing of PMCs. The PLA had a melting temperature of about 148 ^{o}C and a glass transition temperature of about 61 ^{o}C. In the additive industry, PLA (Poly-Lactic Acid) is a widely used biodegradable thermoplastic which is stemmed from abundant natural resources and can be processed from sugar cane, rice, or corn starch. It is also biocompatible and non-toxic and needs relatively lower energy for its use as a starting material in additive manufacturing [62]. The low melting temperature of the PLA makes it less prone to the nozzle clogging or warping problem [63]. In this study, a batch of commercially available PLA filament (MakerBot, USA) was used. The nominal properties of the as-received PLA are represented in Table 3.

Table 3. Properties of the MakerBot PLA filament [61]

Parameters	Values
Heat Deflection (ASTM 648, 66 psi)	52-49°C
Flexural Modulus (ASTM D790, 15 mm/min)	2,600 MPa
Tensile Strength at yield (ASTM D638, 50 mm/min)	62 MPa
Tensile Modulus (ASTM D638, 50 mm/min)	3,600 MPa
Strain at Yield - Elongation (%)	>4.4%
Notched Impact Strength (ASTM D256)	32 J/m

For filler material, the spherical copper powders with a 99.9% purity and the mesh size of -325 were obtained from McMaster Carr retailer (manufactured by AEE, USA). Also, the dendritic copper powders with a mesh size of -325 were obtained from Aldrich, USA, to assess the effect of powder shape on the packing density. The dendritic copper powders are manufactured by the electrodeposition process with a purity higher than that of spherical powders that are usually manufactured by the gas atomization process.

2.2 Overview of PMC Additive Manufacturing

The main stages of this novel additive processing of copper-PLA composite are presented as a flowchart in Fig. 12. At the first step, the PLA was knurled to make surface grooves as carriers of filler material. The knurled filament was then selectively impregnated with the copper filler at specific locations dependent on the designed structure. At the last step, the material was introduced to the extrusion section of the FDM machine for deposition on the substrate for additive manufacturing (3D printing).

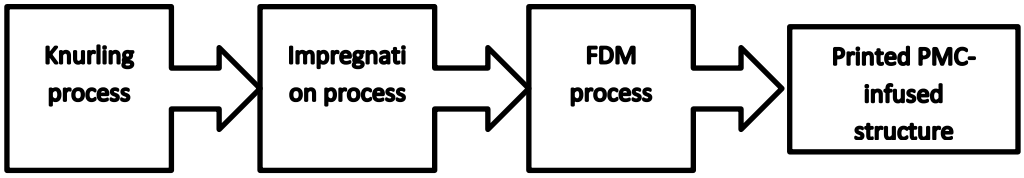

Fig. 12. Three main stages of the PMC additive manufacturing process. The FDM is the main platform of the PMC additive manufacturing process.

All three stages can be ideally integrated into one manufacturing system for automation purposes. A conceptual design of the integrated system is shown in Fig. 13.

2.2.1 Filament Knurling Process

The knurling process is a surface engineering technique where a specific pattern of on the surface of hard rolls is replicated by compressive forces on the surface of a workpiece. The created texture on the surface of materials is conventionally used to increase the surface friction. Also, it improves the appearance of the surface with no change in the chemical or mechanical properties of the bulk material.

The knurling process is used in this study to make grooves on the surface of PLA filaments that will serve as carriers for filler material (copper powder) in the course of additive manufacturing. For this purpose, the filament is introduced in the gap between two idler knurling rolls. Dependent on the features of the knurling rolls, different surface patterns can be replicated on the surface of the filament that is pulled through the gap between the two knurling rolls. The decrease in the gap between the rolls increases the depth of the grooves. The increase in the depth of the grooves is limited by the filament rupture or fracture caused by the excess friction between the material and rolls.

The amount of filler in the PMC structure can be controlled by altering the groove shape/volume and whether the grooves are impregnated with powders or left empty prior to FDM.

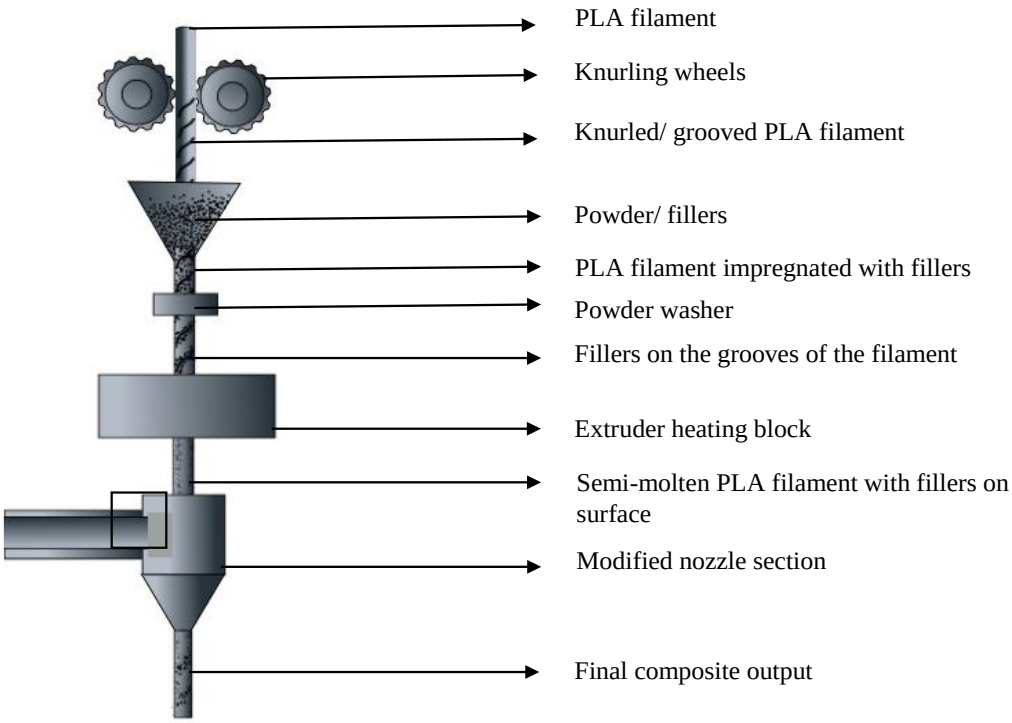

Fig. 13. A conceptual design of an integrated system for additive processing of PMCs.

In order to specify the location of the PMC regions within the 3D structure of the product, the required knurling length must be calculated. The calculation can be facilitated by the use of the G-code files that contain the geometrical data points of a CAD model. The G-code files are generated by the slicer/meshing software, such as Simplify 3D, for the purpose of hardware control in additive manufacturing.

After setting the process parameters such as extrusion speed and temperature, the slicer software calculates the required amount of materials for each layer and generates the G-code file as a guiding map for the disposition of the layers and their sequences.

For this study, two types of knurling rolls with different features, straight line, and helical patterns, were selected. The set up for the knurling process is shown in Fig. 14. The holders of knurling rolls were tied to the vise jaws.

A plastic tube was used to guide the filament through the central region of the gap between the rolls. A digital gauge, with the measurement resolution of 1 □m, was used to control the gap between the rolls. In order to prevent filament jamming in FDM processing, the filament should be knurled without flattening[1]. Before and after the knurling process, the filaments were held inside the vacuum bags at room temperature to prevent exposure to humidity.

[1] Flattening refers to a shape change of the filament from cylindrical shape that can be successfully fed into the FDM process without jamming or shortcoming issues.

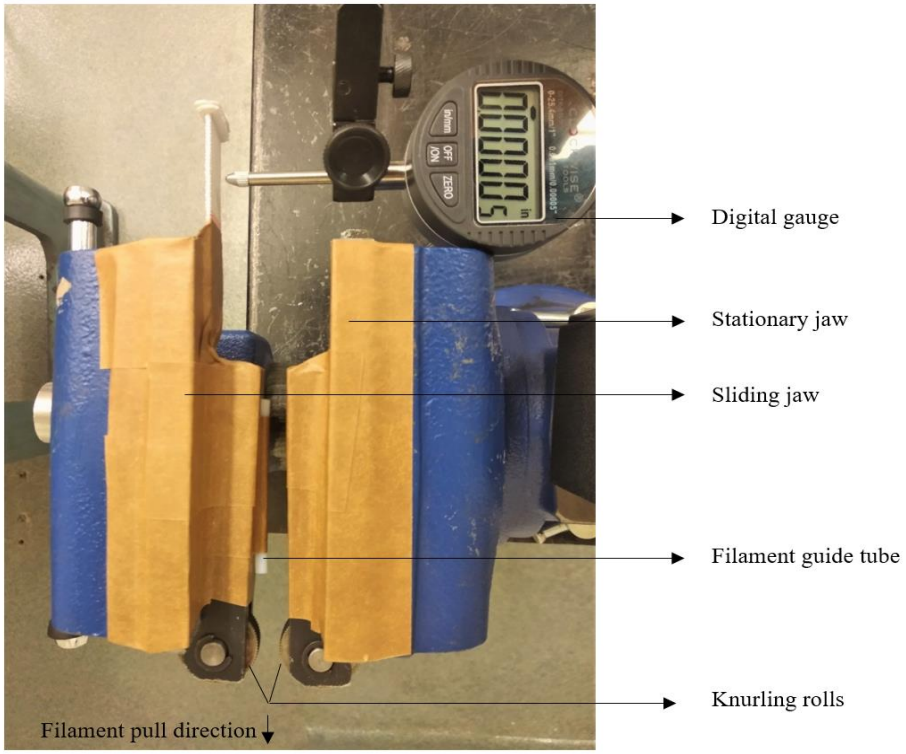

Fig. 14. Filament knurling setup

The depth and volume of the knurled grooves were measured by using a confocal laser scanning microscope (LEXT OLS 4000, Olympus, Japan). The 3D model of the scanned profile of the grooves was analyzed by LEXT OLS analysis software. For reliable image analysis, the image analysis was calibrated by the calculation of a profile with a known volume. For calibration, the surface of a plasticine mold was impressed by an object with a known geometry/volume. The impression was scanned with the laser microscope, and the measurements were confirmed to be within ±10% of the object geometry. Figure 15 shows the plasticine mold with the impression on its surface. Also, the 3D model of the impression is shown in this Figure.

(a)

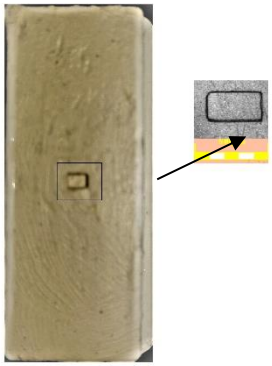

(b)

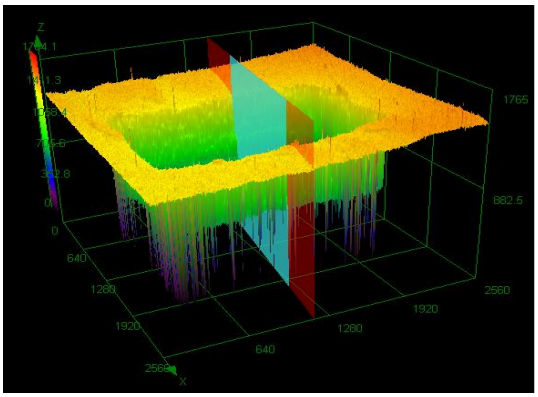

(c)

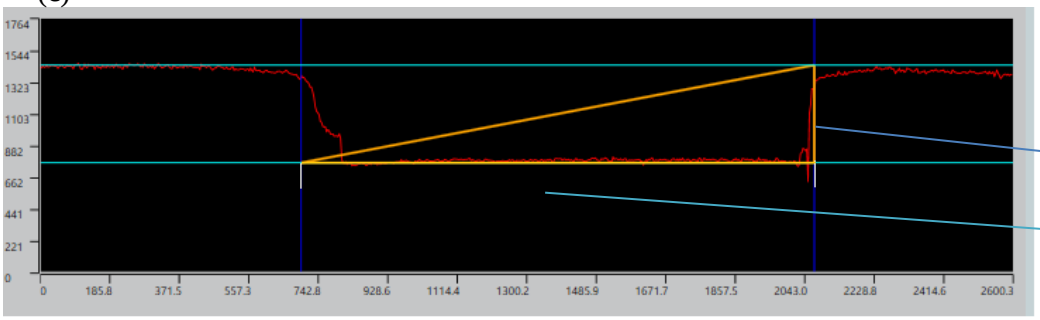

Fig. 15. (a) The plasticine mold with an impression on its surface, (b) a 3D model of the impression that was obtained by using the confocal laser scanning microscope (CLSM), and (c) software analysis for measuring the dimensions of the impression.

2.2.2 Filament Impregnation

The powder particles were used to impregnate the knurled filament in two conditions: as-received and preprocessed conditions. for preprocessing, the copper powders were emulsified into liquid starch before introducing them to the grooved region. The starch was prepared by boiling rice grains with water for about 15 minutes. When the water got steamed, the rice grains were removed, and the remaining water was heated again until the color changed to white, which indicated a viscose liquid starch. The liquid was cooled down and mixed with copper powders prior to the impregnation process. The nature of the starch helped the copper powders to adhere to each other more densely compared with the as-received powder condition. The starch-powders mixture was conducted on a trial base with no measurement of the proportionality of ingredients. The dynamic viscosity of the starch was measured as 477 mPa.s by using a rotational rheometer (NDJ-5S, China) at room temperature with a rotational probe speed of 6 RPM. The starch was a shear-thinning liquid as its viscosity reduced by increasing the rotational speed of the rotor. The density of the starch at room temperature was measured as 0.99 g/cm3. After impregnation, a dry lint-free cloth was used manually to remove the additional fillers from the outside of the grooves.

A. Length Estimation for Impregnation

The required area/region of the filament to be impregnated was calculated from the developed G-code associated with the CAD model in the slicing step. A commercially available slicer software, Simplify 3D, was used to generate the G-code and calculate the total length of the filament for printing. The objective was to manufacture a 3D printed sample, with a length of 90 mm, that has a 20 mm PMC section in the middle of its length. The required length of the filament for the PLA and PMC regions were determined by Simplify 3D software. The samples were designed to have one layer in their thickness direction.

The knurled filament was covered by removable adhesive tapes outside the regions of impregnation. After impregnation and cleaning, the cover tapes were removed. Figure 16 shows knurled filaments after impregnation with the spherical copper powders in their as-received and starch-processed conditions.

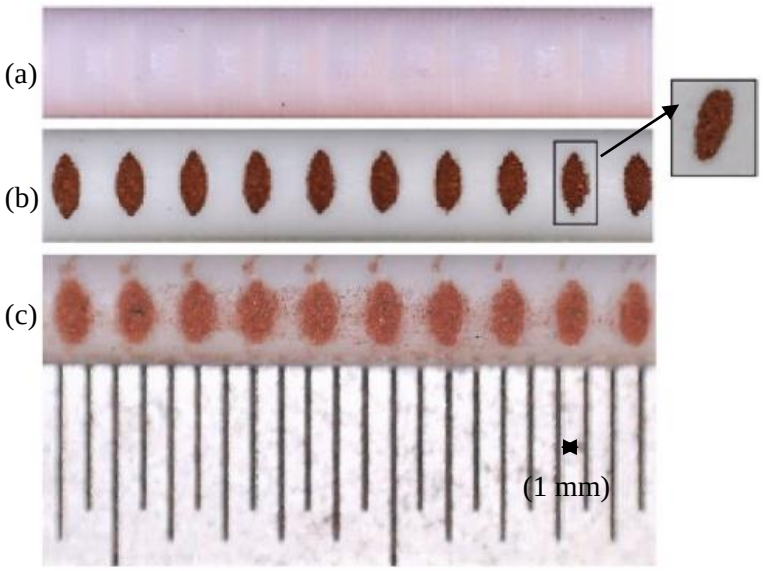

Fig. 16. Knurled filament (a) before impregnation and after impregnation (b) with starch-processed powders and (c) with as-received spherical powders.

B. Mass Measurement of Impregnated Filament

The mass of the filaments before and after impregnation was measured to calculate the packing density of different powder types that are used for this study.

A protocol for measuring the copper mass is presented in Fig. 17. In the first step, a piece of knurled PLA filament was taped to a polymer film as a substrate. The total mass of this knurled filament with its substrate was measured by using a precision balance (Mettler-Toledo, Model ME54TE, USA) with a measurement resolution of 0.1 mg. After this initial measurement, a known number of grooves were impregnated manually. The powders outside the grooves were carefully cleaned

following the procedure detailed earlier. Then the mass of this impregnated filament on the substrate was measured. Finally, the impregnated filament was removed, and the mass of the taped substrate was repeatedly measured to consider any additional powder particles that could remain on it during the impregnation process. Following the measurement, the mass of the powder particles for ten grooves was calculated.

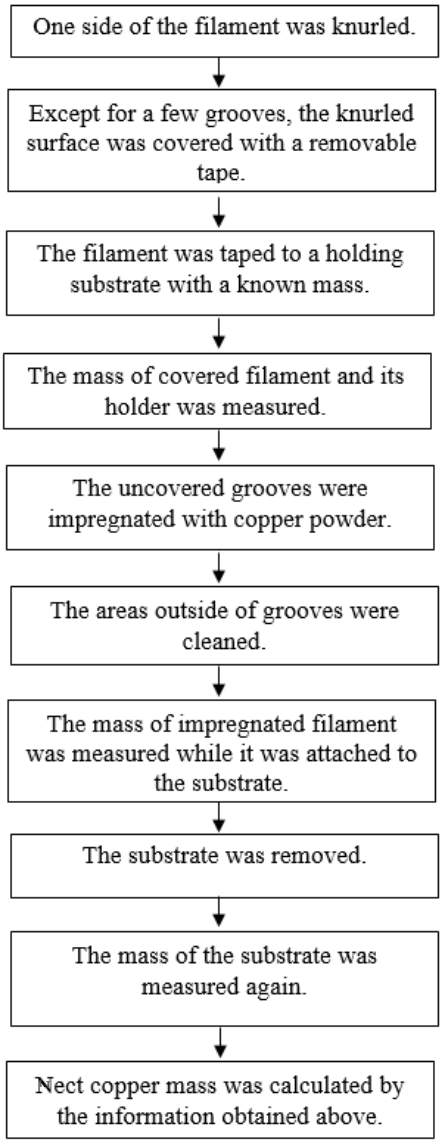

Fig. 17. A flowchart of the mass measurement protocol for calculation of copper mass inside of grooves after the impregnation process.

2.3 Sample Preparation (FDM Processing)

A commercially available FDM printer (Replicator Mini+, MakerBot, USA) was utilized for the additive manufacturing of PLA samples with the PMC region(s).

One set of samples was prepared by only using the as-received PLA filament. The second set of samples was manufactured through the developed composite processing technique. The samples had a PMC region that was sandwiched between two PLA regions, as shown in Fig. 18. For this set of samples, the filament was impregnated with spherical shape powders in two conditions: as-received and starch-emulsified, as described earlier in this chapter.

The nozzle orifice diameter was 0.8 mm, and the layer height was set at 0.6 mm. The extrusion temperature was maintained at 215±3°C during printing. The nozzle and the build plate were moving along the width and length direction of samples, respectively. The relative humidity and room temperature were measured around 50% and 22°C, respectively.

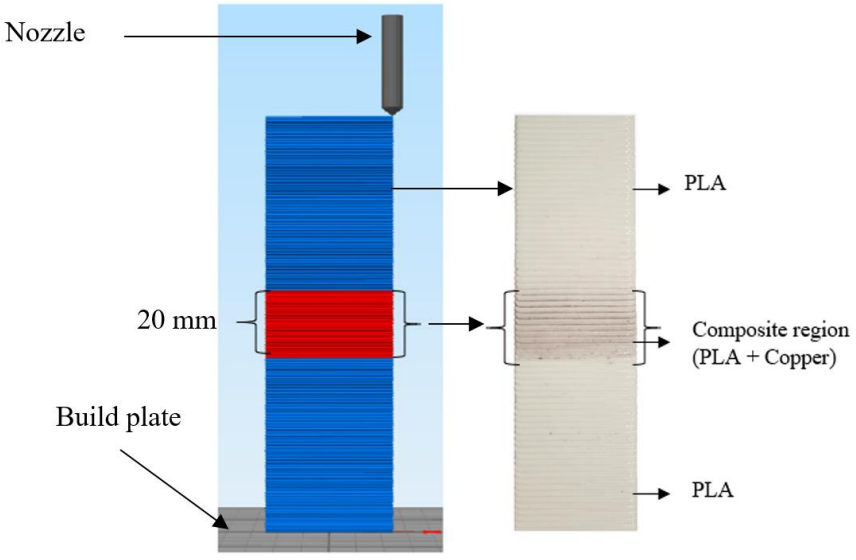

Fig. 18. A Simplify 3D model (left) and a picture of a printed sample with a PMC region in the middle of its length direction (right).

2.4 Post Manufacturing Treatments

In addition to as-printed samples, two more sets of samples were prepared by two post-manufacturing processes of microwave and electrical furnace treatments. These treatments will be discussed below.

2.4.1 Microwave Treatment

Microwave heating allows for the fast processing of materials compared to conventional heating processes and generally provides improved sintering kinetics [64]. The key characteristics that differentiate microwave heating from traditional methods are higher rate of energy transfer, rapid and selective heating of materials. The MW heat treatment can result in reduced processing temperature and time, leading to higher productivity and a reduction in energy use [65].

Depending on the nature of the material, an electromagnetic microwave can be mainly reflected, absorbed, or transmitted by the materials [66]. Due to a very low dielectric loss factor, the pure insulators have no or negligible energy absorption, and they are, therefore, transparent to microwave energy. The prohibited band in pure insulators is thick, limiting any movement of electrons forming conduction band to valence band, so no polarization is possible [67]. In metallic powders, the skin depth is comparable to their size, which allows them to couple with MW energy. However, the metals' skin depth is very small, and metals are mainly considered reflective in their interaction with MWs [68]. The classification and behavior of different materials under microwave exposure is shown in Figure 19.

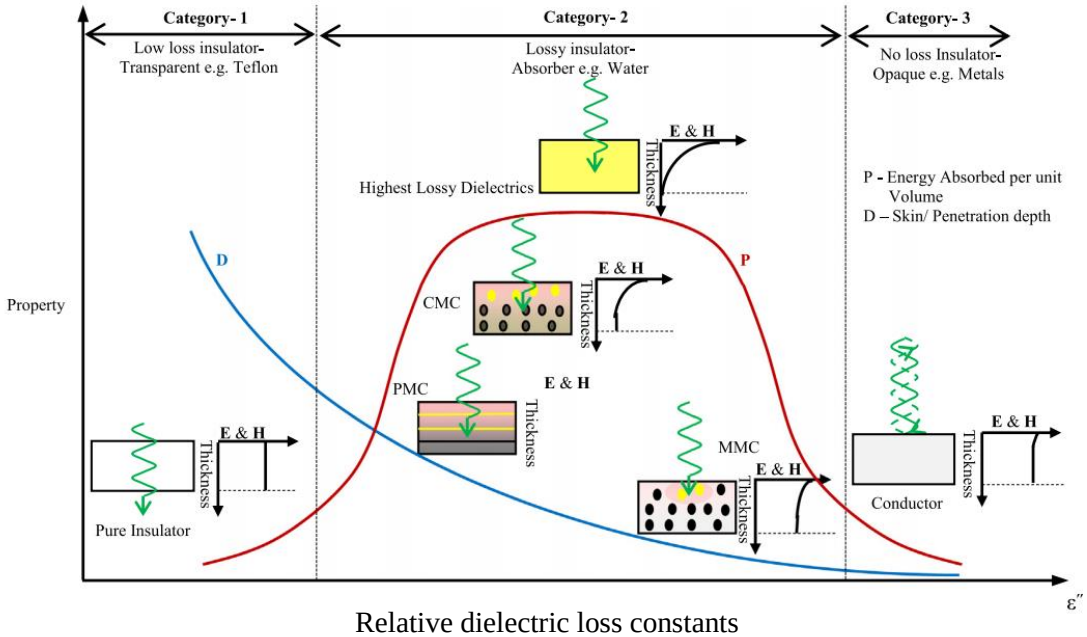

Fig. 19. Microwave interaction with different materials [68]

Yarlagadda et al. [69] utilized concentrated microwave energy to investigate the joining mechanism of engineering thermoplastics. A detailed review was published by Ku et al. [70,71] on characterizing different fiber-reinforced thermoplastic composites and the effect of MW frequency on their tensile properties. Singh et al. [72] investigated the MW interaction with the natural fiber-reinforced biopolymers and its positive effects on the faster polymerization process. Sweeney et al. [73] used microwave heating to increase the bonding between 3D printed CNT/PLA composite. They achieved a 275% increase in the fracture strength in comparison to the non-treated parts. A similar study was conducted by Wang et al. [74] to investigate the effect of MW on SiC coated PLA composite parts. The MW treated composite parts showed a 51% increase in tensile strength.

For the analysis of microwave interaction with materials, the Maxwell equations can be used [65].

$$\nabla \times \mathbf{E} = \frac{\partial B}{\partial t}, \nabla \cdot \mathbf{B} = 0, \nabla \times \mathbf{H} = \frac{\partial D}{\partial t} + \mathbf{I} \text{ and } \nabla \cdot \mathbf{D} = \rho \quad (1)$$

Here, B and D represent the magnetic and electrical flux density vectors. The parameters I, H, E, and ρ represent the current density vector, magnetic field vector, electric field vector, and electrical charge density, respectively. The parameter t represents time. The microwave electric field exerts a force on the charged particles present in the compound. When the charged particles have limited movement, they can merely oscillate within the electric field. This phenomenon is called dielectric polarization and can be represented as a combined effect of four components [75].

$$\alpha_t = \alpha_i + \alpha_d + \alpha_a + \alpha_e \quad (2)$$

α_t = total dielectric polarization, α_i = interfacial polarization, α_d = dipolar polarization due to polarization of permanent dipoles, α_a=atomic polarization caused by the relative motion of the atoms and α_e= electronic polarization generated from the polarization of electrons surrounding the nuclei. Another two factors that play a significant role in MW processing of dielectric materials are dielectric loss (loss tangent) and complex relative permittivity [71]. These parameters are defined as

$\tan\delta = \varepsilon''/\varepsilon'$ Loss tangent, (3)-A

$\varepsilon = \varepsilon' - i\varepsilon''$ Complex relative permittivity (3)-B

while ε' and ε'' represent relative dielectric, and relative dielectric loss constants, respectively. Loss tangent describes the ability of dielectric material to turn the influx energy into heat, and the complex relative permittivity defines the amount of dissipated energy from the source and the amount that enters the sample.

The PLA is a dielectric material with low absorption of microwaves at room temperature. In contrast, the copper powders are reflective with a small depth skin at which the microwave can penetrate and heat the metallic powder. In this study, an Amana industrial-grade microwave oven

(Model RC30S2, USA) was used to expose the printed samples. The oven can provide a maximum of 3kW power with a microwave frequency of 2.45 GHz. The samples were placed at a prespecified region inside the microwave chamber, close to the oven wall, one after another. A research publication [76] showed that for electrically conductive materials, the efficiency in MW absorption increases with the magnetic field of the microwaves, which is highest close to the oven wall. A picture of the microwave oven is shown in Fig. 20. Immediately after exposure with 3kW MW for 30, 60, 75, and 90 seconds, the temperatures were measured using an infrared handheld thermometer with a measurement accuracy of ± 1.9 ºC.

Fig. 20. A picture of the Amana microwave oven used for this study. A sample is shown in the oven chamber close to the wall.

2.4.2 Electrical Furnace Treatment

During the microwave exposure, the samples were placed on the surface of the oven, and therefore, there were the effects of external heat convection and conduction. In order to exclude these effects for the analysis of the properties of MW-exposed samples, another set of printed samples were treated in an electrical furnace with the same soaking time of MW-exposed samples. The temperature of furnace treatments was devised based on the infrared measurement of the highest samples temperature that was measured immediately after MW exposure.

For the furnace treatment, an electrical furnace chamber (Carbolite Gero, CWF1313, England) was used. The temperature and exposure time for furnace-treating the printed samples are represented in Table 4.

Table 4. Temperature and soaking time of furnace heat treatment of the samples

Temperature (ºC)	50	70	90	125
Exposure time (s)	30	60	75	90

2.5 Fracture Test (Uniaxial Tension)

An INSTRON machine (Model 5982, USA) equipped with a 100 kN load cell was used for mechanical testing of the samples to assess their fracture behavior under uniaxial tension. The accuracy of the measurements for load and displacement was ±0.5% of reading values and ±1μm, respectively. The area under the load-displacement curve was calculated as the fracture energy. The fractured samples were used for fractography and DSC analysis.

2.6 Fractography

The thickness of the samples at the fracture area was measured by using the confocal laser scanning microscope. For this microscope, the presence of a 405nm short-wavelength laser and a high aperture objective lens offers a minimum of 0.12μm X-Y resolution for performing submicron measurements on the sample surface. A precise linear stage of 0.8 nm resolution and software algorithms enables the height scanning resolution of 10 nm. The fracture surface of the samples was scanned by the laser, and the images were captured by using the 5X and 10X objective lenses. Image analyzer software (MIPAR, USA) and ImageJ (NIH, USA) was used to calculate the voids percentage and their sizes and distribution at the fracture area.

CHAPTER III

RESULTS AND DISCUSSIONS

Three main stages of the PMC additive manufacturing were described in detail in the previous chapter. In the filament knurling stage, the size and pattern of the grooves on the firmament surface are important process parameters for the determination of the spatial architecture of PMC in the printed structure. In the impregnation and cleaning stage, the packing density of powders is considered as an important factor that determines the amount of copper powder and its distribution in the polymer matrix at PMC regions. Finally, after the FDM process, the properties of the structure need to be characterized for further development of the process.

3.1 Depth and Volume of Grooves Made in the Filament Knurling Stage

In this study, two different sets of knurling patterns (helical and straight line) were used to prepare the knurled filaments for mass measurement analysis of the intruded powders. The straight-line pattern was also used for PMC manufacturing. Three different knurling gaps were devised to make the shallow, intermediate, and deep grooves for both types of patterns. For the helical knurled filaments, the measurement of depth at the center of grooves revealed that the depth of grooves increased with a geometrical ratio of 1.2.

For the helical knurled filaments, the measurement of depth at the center of grooves revealed that the depth of grooves increased with a geometrical ratio of 1.2. For the grooves in the straight-line pattern, the ratio of depth was 1.1 and 1.3, for intermediate and shallow grooves, and deep and intermediate grooves, respectively. The 3D models of the grooves with different patterns and sizes were obtained by using the CLSM (see Fig. 21).

The depth and volume of the grooves are reported in Table 5. For the helical knurling, the volume increased by 40% and 58%, respectively, for intermediate and deep grooves in comparison with smaller groove types. For the straight-line pattern, the increase in volume from shallow to intermediate grooves was just 11% compared with an increase of 93% for deep grooves in comparison with intermediate ones.

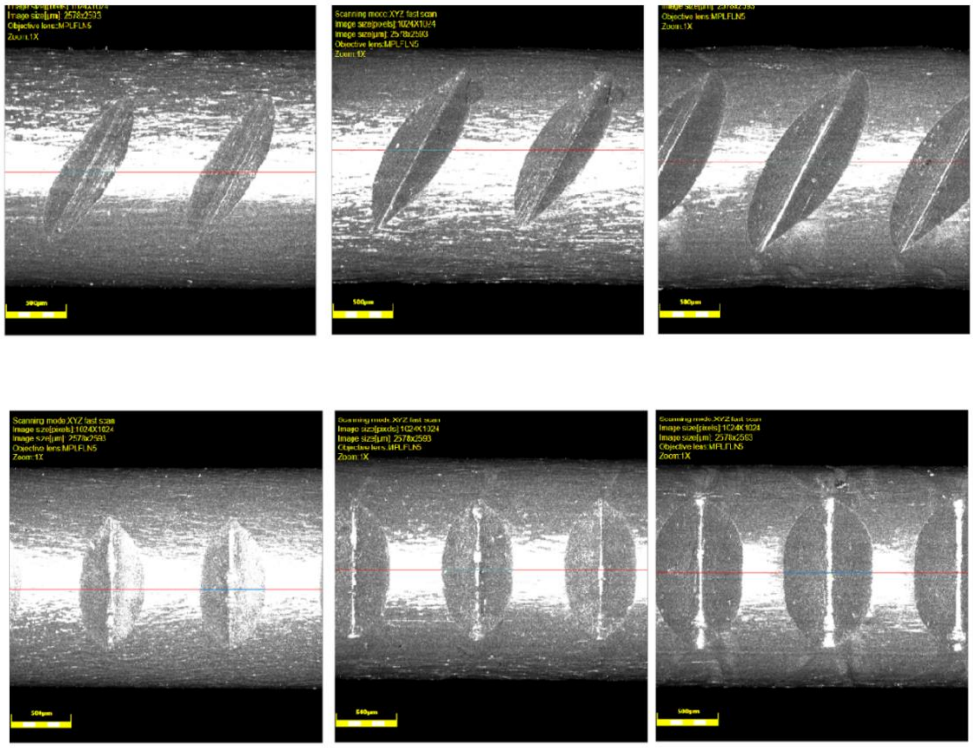

Fig. 21. Microscopic images show the helical (top) and strain-line (bottom) grooves with different depths. From left to right, the depth of grooves increases.

Table 5. Depth and volume of knurled grooves

Type	Shallow groove		Intermediate groove		Deep groove	
Knurling pattern	**Helical**	Straight-line	**Helical**	Straight-line	**Helical**	Straight-line
Depth (mm)	**0.225**	0.211	**0.270**	0.228	**0.331**	0.290
Volume (mm^3)	**0.505**	0.471	**0.706**	0.523	**1.112**	1.010

3.2 Packing Density of Copper Powders after Impregnation

Two different shapes (dendritic and spherical) of copper powder with two different conditions (with starch and without starch) were used for the impregnation process. Both powder shapes had the same mesh number of 325, with a sieve size opening of 45 microns. The mass of powders in the grooves after impregnation is reported in Fig. 22.

The increase in depth (volume) of the grooves, and the use of starch significantly increased the mass of occupied grooves. The impregnation with spherical powders resulted in a higher mass of occupied grooves in comparison with dendritic powders in all groove types and impregnation conditions.

The shape and size of both the particle and container play a significant role in determining the particle packing density and related porosity [77]. The packing density of the powders is inversely related to the volume fraction of porosity. The volume fraction of porosity inside the grooves after the impregnation and cleaning process is shown in Fig. 23. The results show that for both groove patterns in all depth conditions, the highest and lowest volume fraction of porosity was observed for the non-starch dendritic and starched-spherical powders, respectively. Also, the porosity volume percentage was highest for deep grooves in all impregnation conditions. One can infer that

the rate of increase in groove volume surpassed the rate of increase in mass for deeper grooves, resulting in a high porosity percentage.

A comparison between the results reveals that the decrease in the depth of the grooves can be more effective than the change in the powder shape from dendritic to spherical for increasing the packing density. The powders with the dendritic shape pack with higher porosity because the dendritic branches create obstacles and prevent the other particles filling the air gaps. In contrast, the small size spherical powders can slip and occupy the spaces between larger ones during impregnation and cleaning processes. As a result, spherical powders showed lower volume porosity in comparison with corresponding dendritic powders.

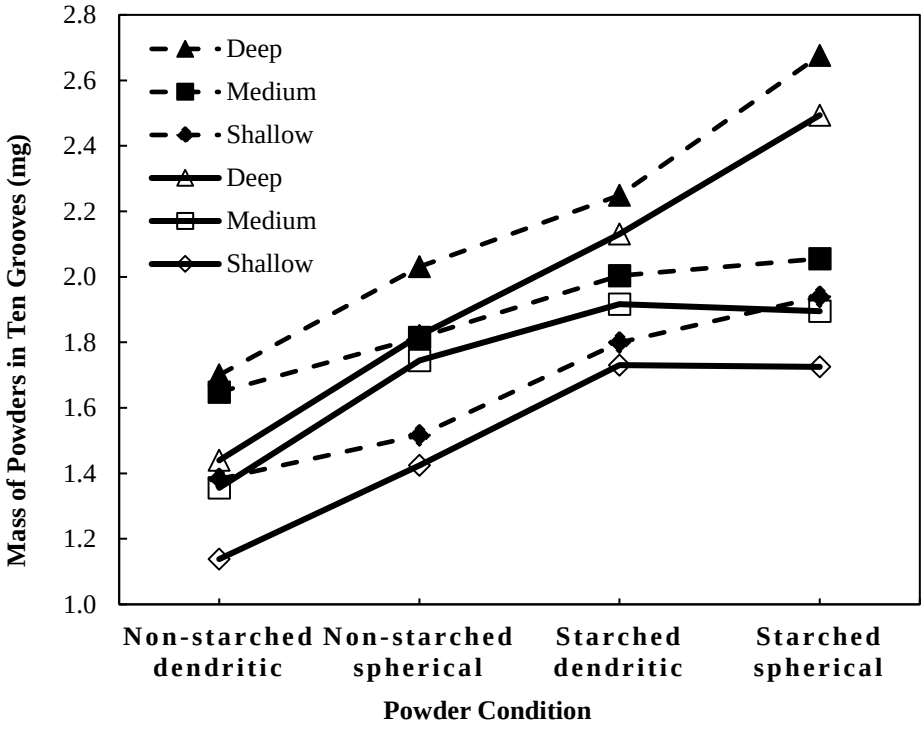

Fig. 22: Mass of powders in ten grooves after the impregnation process. The solid lines represent the non-starched condition, and dashed lines represent the starched condition.

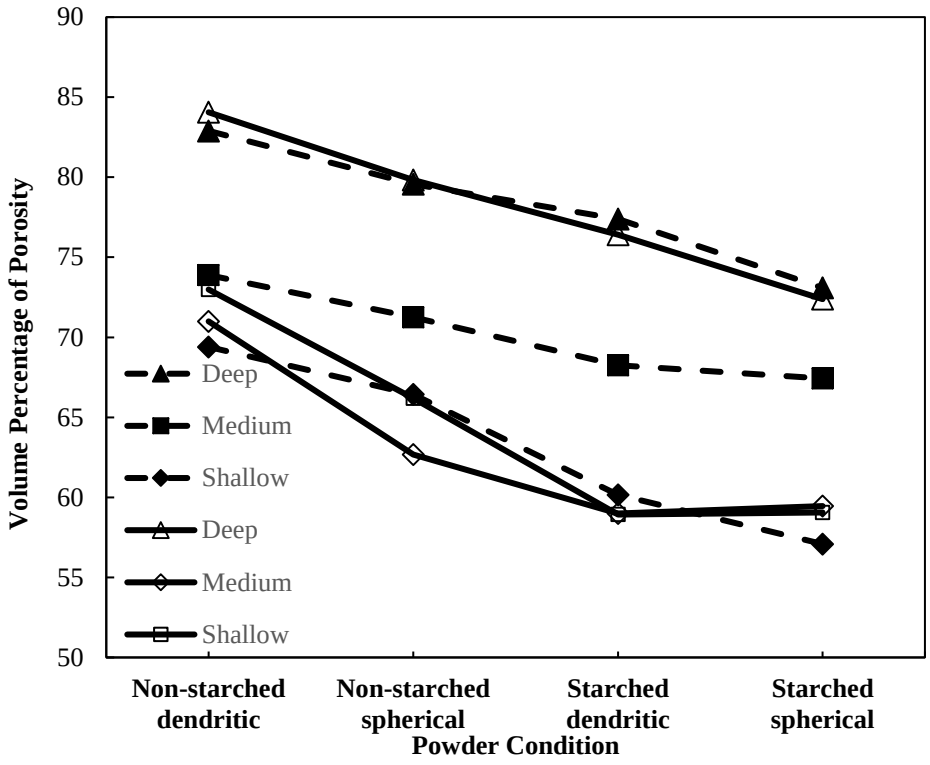

Fig. 23. The volume percentage of porosity inside of grooves after impregnation with copper powders. The solid lines represent the non-starched condition, and dotted lines represent the starched condition.

3.3 Characterization of FDM Processed Composites

3.3.1. Fracture Properties of As-printed Samples

Uniaxial tensile tests were conducted to analyze the interlayer fracture energy of the printed samples. At least five samples were tested at each condition. Fig. 24 represents a typical force-displacement curve, which is obtained from the uniaxial tension test on the printed samples. As shown, the resistance force was increased to a maximum amount before a sharp drop due to the fracture. The fracture was brittle and occurred at the interlayer area for all sample conditions. Three different sample conditions were tested: as-printed (PLA, non-starched-Cu/PLA, Starched-

Cu/PLA), MW heat-treated starched-Cu/PLA, and furnace heat-treated starched-Cu/PLA conditions.

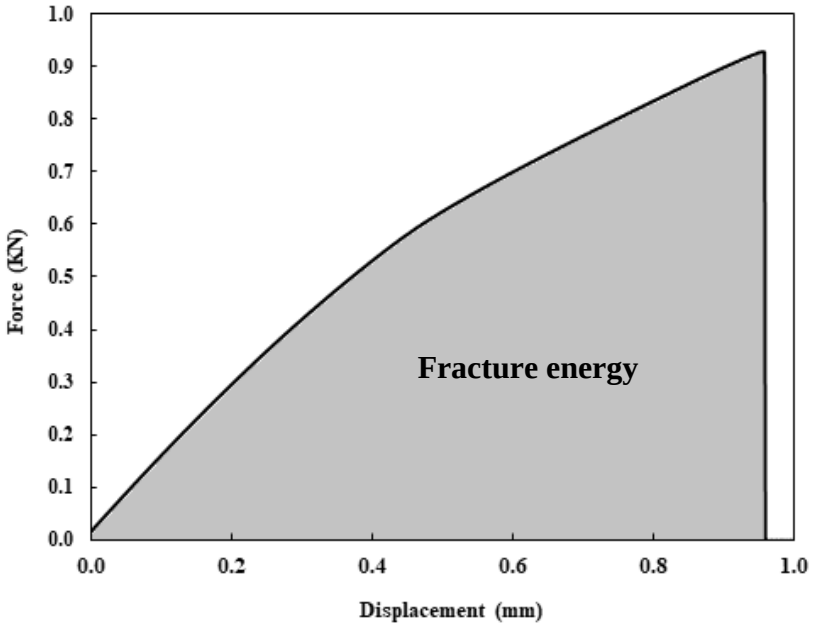

Fig. 24. A typical force-displacement curve obtained from uniaxial tensile test

The area under the force-displacement curve represents the amount of required energy for the fracture [78]. This area was calculated by integrating a polynomial equation of a curve, which was fitted (with an R-squared value of 1) to the force-displacement data points. The normalized fracture energy was calculated by normalizing the fracture energy with respect to the contact area (contact thickness × unit width).

The fracture thickness of the samples was measured with an accuracy of ±1 μm (see Table 6). Since fracture was brittle for all cases, the fracture thickness was considered to be the contact thickness between the layers prior to the uniaxial tension test.

Table 6. Fracture thickness (mm) of the 3D printed samples.

As-Printed			MW-treated Starched Cu/PLA				Furnace-treated Starched Cu/PLA			
PLA	Non-starched Cu/PLA	Starched Cu/PLA	30 s	60 s	75 s	90 s	50 °C-30 s	70 °C-60 s	90 °C-75 s	125 °C-90 s
1.027	1.144	1.180	1.188	1.220	1.201	1.184	1.224	1.175	1.171	1.187

The larger fracture thickness of composite samples is attributed to the presence of copper powders in the PLA structure. The image analysis of the fracture area revealed that the area fraction of copper was 1.56 and 9.9% for non-starched and starched composite samples, respectively. Also, the copper particles promoted the nucleation and refinement of the voids at their interface with PLA (see Fig. 25). The image analysis of the fracture area showed that the presence of copper powders increased area percentage of imperfections (voids and cracks) from 33% for PLA to an average of 57% for composite samples.

For PLA samples, the interlayer fracture could occur anywhere with no preferred location in the gauge length of the samples. However, for all other samples, the interlayer fracture occurred in the composite region, as shown in Fig. 26. The interlayer strength of the PMC region in the printed structure was weaker than that of PLA regions, and therefore, the PMC played a role as a predetermined fracture zone.

(a)

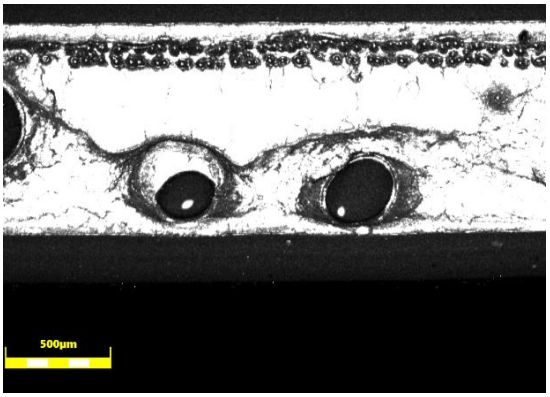

(b)

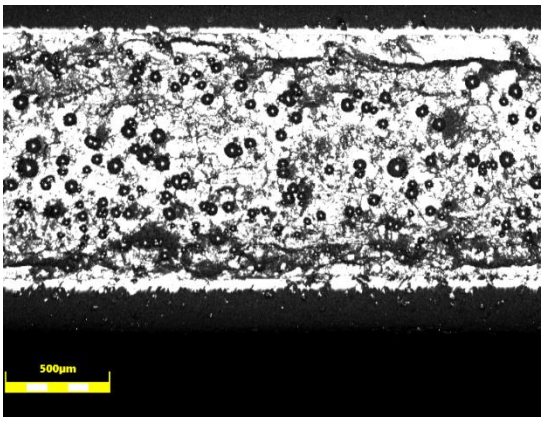

(c)

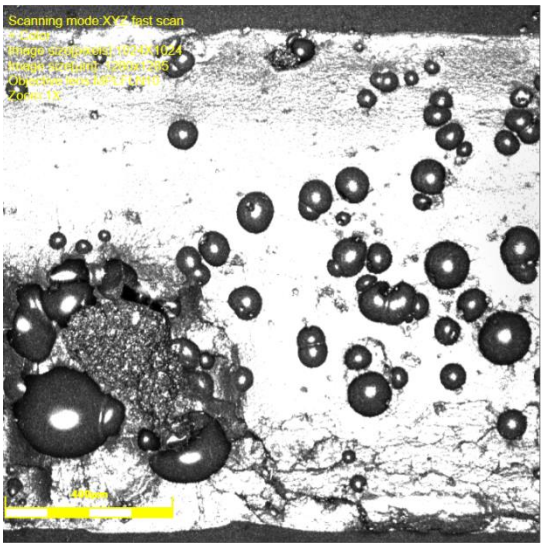

Fig. 25. The fracture surface of as-printed PLA (a), and starched Cu/PLA composite (b) is shown. The presence of voids at the surface of copper particles indicates the role of particles as the nucleating agent for voids (c).

The interlayer fracture energy of the as-printed samples is shown in Fig. 27. The error bars represent the range of data. The as-printed PLA samples showed about 53% and 108% higher fracture energy than the non-starched-Cu/PLA and starched-Cu/PLA samples, respectively. In general, the change in the fracture energy can be attributed to different factors, including area percentage of imperfections (voids and cracks), the size and distribution of voids, degree of crystallinity, and residual stress. These factors can be either process-induced or materials-induced parameters.

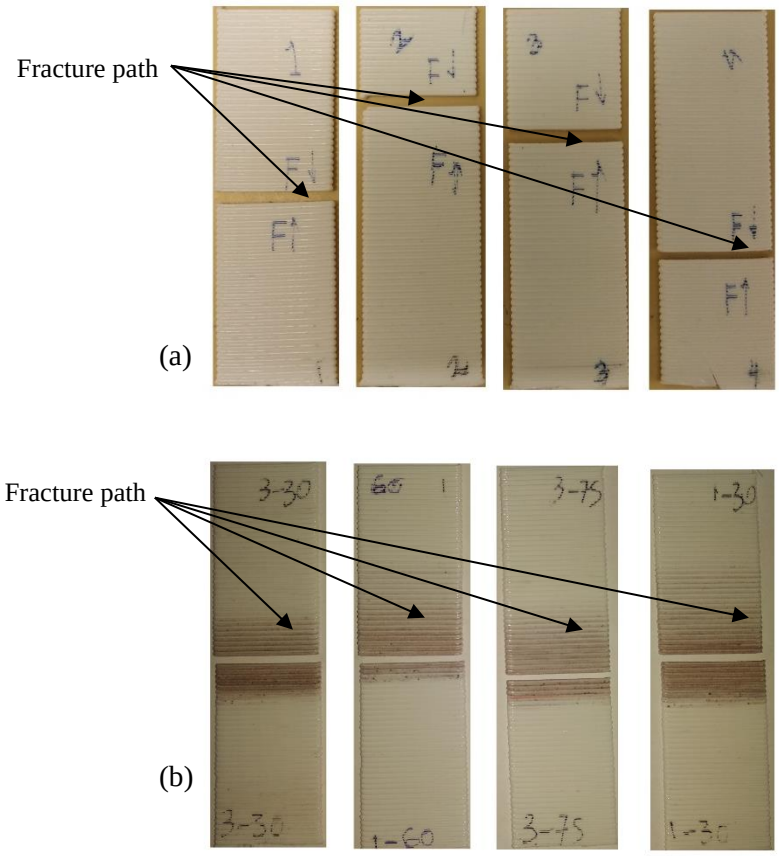

Fig. 26. The images of samples of (a) PLA with different locations for fracture path, and (b) composite samples with fracture path at PMC region. The red color indicates the presence of copper powders in the structure.

In comparison with PLA samples, the composite samples had more area percentage of imperfections (about 73%), and therefore, the fracture energy for composite samples is less. The fracture energy of starched samples was 26% less than that for non-starched samples. Although the area percentage of imperfections was comparable for these two cases, the average size of voids was 55 μm for starched samples in comparison with 62 and 67 μm, respectively, for non-starched composite and PLA samples. Table 7 summarizes the average and standard deviation of void sizes obtained from image analysis of the fracture area. The results show most uniformity in void size distribution for starched composite samples. In comparison with non-starched samples, the higher uniformity in void size for starched samples can be indicative of a more uniform distribution of voids at the fracture area. The voids and their interface with PLA induce anisotropy in properties, including fracture strength. The voids reduce the contact area, and their interphase with PLA and copper matrix raises the stress concentration factor and weakens the fracture strength. The presence of copper particles with significant differences in mechanical and physical properties can be considered as a cause for the development of residual stress inside the printed structure and at the interlayer areas of manufactured samples. As an example, the amount and rate of heat expansion and contraction are different for copper and PLA. During the deposition and cooling process in additive manufacturing, the difference in properties can be considered the cause for the development of tensile residual stresses and potentially weaken the bond between the layers in 3D printed structures. Also, the geometrical incoherency at the interface between voids, copper, and PLA and the presence of micro-cracks at the interface can change the stress state during fracture tests from uniaxial to triaxial loading condition. This change in the stress state may also be considered as one of the accumulative reasons for the weakening of interlayer bonds in composite samples.

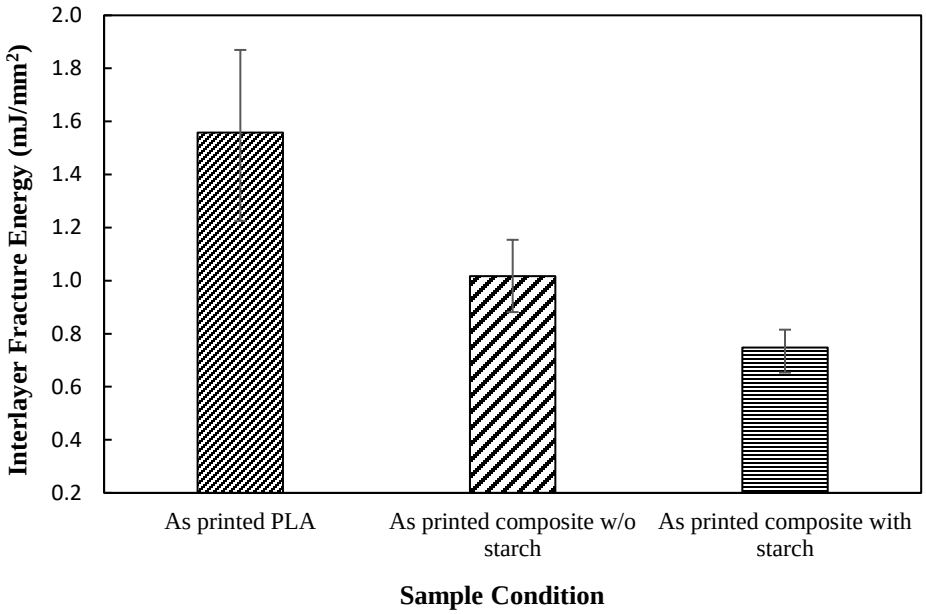

Fig. 27. Comparison of interlayer fracture energy of the as-printed samples.

Table 7. The average and standard deviation of sizes of voids at fracture area for as-printed samples.

	As-Printed samples		
	PLA	Non-starched Cu/PLA	Starched Cu/PLA
Average (μm)	67	62	55
Standard deviation	37	31	17

3.3.2. Effects of Post-Manufacturing Treatments on Fracture Properties

PLA has a low dielectric loss factor at room temperature, and therefore, it is considered mainly transparent to the microwave (MW), as described in section 2.4.1. The copper powders are highly reflective and have a small skin depth that can absorb the MW and heat up. For both materials, the absorption of MW will increase with increasing temperature [76].

The starched-Cu/PLA samples were exposed to a microwave (with a frequency of 2.45 GHz and power of 3 kW) for four different exposure durations of 30, 60, 75, and 90 seconds. The normalized fracture energy values for MW-treated samples are compared with the fracture energy of non-treated composite samples in Fig. 28.

The fracture energy was maximum for the samples with an exposure time of 75 seconds. The statistical analysis (t-test with a 95% confidence interval) revealed that the MW exposure for 30 and 60 seconds did not significantly change the fracture energy. However, the samples with 75 seconds of exposure showed a significant jump of 26% in the average fracture energy in comparison with samples that were exposed for 60 seconds. Further increase in the exposure time to 90 seconds decreased the fracture energy but not lower than that for the samples with 60 s of exposure. The statistical analysis showed that the exposure durations of 75 and 90 seconds increased the fracture energy significantly in comparison with other MW-treated and non-treated composite samples. The fracture energies of samples with 75 seconds of MW exposure was comparable with the fracture energy of as-printed non-starched composite samples.

As detailed in chapter 2, the MW treatment involved conduction and convection types of heat transfer due to the contact of samples with MW chamber surfaces and the circulation of air within the chamber. In order to decouple the effects of heat conduction and convection on the fracture properties of MW-treated samples, the composite samples were also heat treated by using a

conventional electrical furnace at the highest temperature of samples after MW exposure. The fracture energy values of furnace-treated samples are shown in Fig. 29.

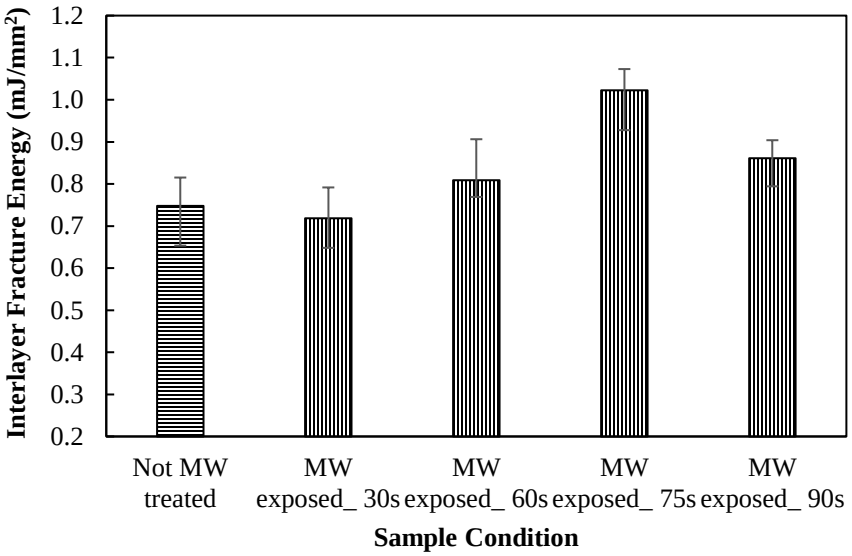

Fig. 28: Comparison between MW-treated starched-Cu/PLA samples with as-printed counterparts

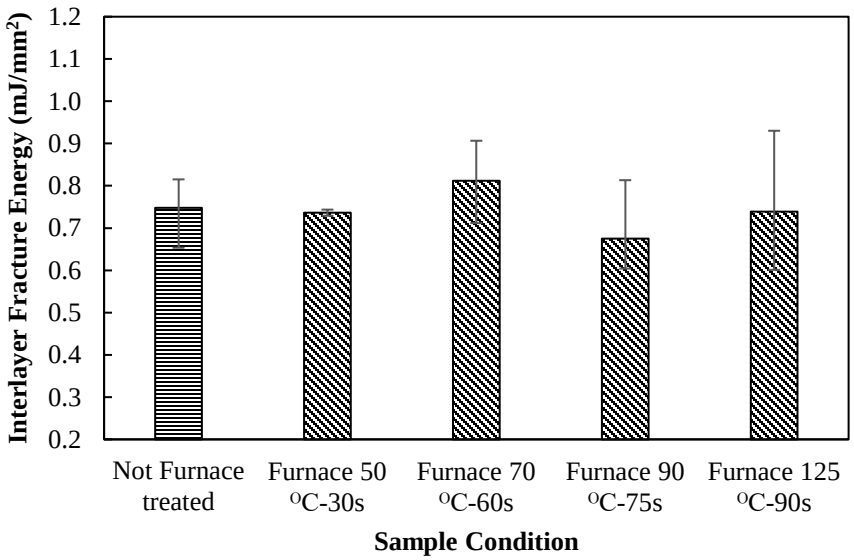

Fig. 29. Comparison between furnace-treated starched-Cu/PLA samples with as-printed counterparts.

The statistical analysis proved that the furnace treatment did not significantly change the fracture energy relative to that for as-printed composite samples. Thus, it can be inferred that the increase in fracture energy for the MW-treated samples can be attributed to the effect of microwave and its interaction with constituent materials in the composite structure.

As presented in Table 8, the area percentage of imperfection for treated conditions was comparable with non-treated composite samples. The average size of the voids is presented in Table 9. In general, one may argue that the amount, size, and uniformity in the distribution of voids interactively affect the fracture properties. As discussed for as-printed (non-treated) conditions, the smaller size and more uniform distribution of voids may be partially the reasons for decreasing the fracture strength. For treated samples, if the change in fracture energy was not significant, there can be two possibilities. If the treatment process did not cause any change to the fracture properties, then one can infer that the fracture strength was insensitive to the difference in the area percentage of imperfections, void sizes, and their distribution in reported range (see Tables 8 and 9). The other possibility can be the neutralizing effects of the treatment process on the effects of changes in the area percentage of imperfections, void size, and distribution. The bold example is the Furnace-treated samples at 125 ^{O}C for 90 seconds. For this sample condition, the area percentage of imperfection decreased for this sample to 44%, and the average void size was larger in comparison with non-treated composite samples. As these parameters suggest higher fracture energy for this condition, no significant difference with non-treated samples might be due to a neutralizing effect of the furnace treatment process. As discussed earlier, the development of residual stress or an increase in the degree of crystallinity can be two candidates for such neutralizing effects.

For MW-treated samples under 90 seconds of exposure, the larger size of voids with less uniform distribution (inferred from high standard deviation) might be responsible for the increase in fracture energy in comparison with the results for MW-treated samples under 30 seconds of exposure. Since the additive manufacturing parameters were the same for these two sample conditions, one may

infer that the MW interaction with copper powders was favorably increased the void sizes by coalescence of voids. If this was the case, the mechanism behind this phenomenon remains unanswered.

Table 8. Area percentage of imperfections (voids and cracks) at fracture area for different sample conditions.

Non-treated			MW-treated				Furnace-treated			
PLA	Non-starched Cu/PLA	Starched CU/PLA	30 s	60 s	75 s	90 s	50 ^{O}C-30 s	70 ^{O}C-60 s	90 ^{O}C-75 s	125 ^{O}C-90 s
33	57	57	53	56	54	56	57	61	58	44

Table 9. The average and standard deviation of sizes of voids at fracture area for the treated samples.

	Treatment conditions								
	Non-treated	MW-treated				Furnace-treated			
	N/A	30 s	60 s	75 s	90 s	50 ^{O}C-30 s	70 ^{O}C-60 s	90 ^{O}C-75 s	125 ^{O}C-90 s
Average (μm)	55	67	57	58	69	62	67	54	70
Standard deviation	17	22	18	18	33	20	24	17	37

Since the area percentage of imperfections and size and distribution of voids are similar to non-treated samples for MW-treated samples under 75 seconds of exposure, the increase in fracture energy is attributed to the effect of microwave interaction with the material. In order to determine how the constituent materials, PLA or copper, could interact with microwave, a set of PLA samples were subjected to MW and furnace treatments followed by uniaxial tension tests. As shown in Fig. 30, the comparison between the fracture energy values for as-printed composites and treated ones did not yield in a statistically significant difference. One can conclude that the copper powders and their interaction with microwaves were responsible for the increase in the fracture energy of MW-treated samples.

The microwave heating of copper powders at their skin depth is speculated to affect the fracture energy with two possible mechanisms. While the exposure time was not as enough as 90 seconds for the coalescence of voids, the local heating at the interface of particles with PLA helped to strengthen the bond between constituents.

The relief of residual stresses or increasing the contact area can be the causes of the bond strengthening mechanism. The other mechanism can be through a decrease in the degree of crystallinity at the interface between copper particles and the PLA matrix. After surface heating of particles and in the cooling stage, the local rate of cooling is higher due to the presence of copper particles. As a result, the degree of crystallinity decreases, and the fracture energy would increase.

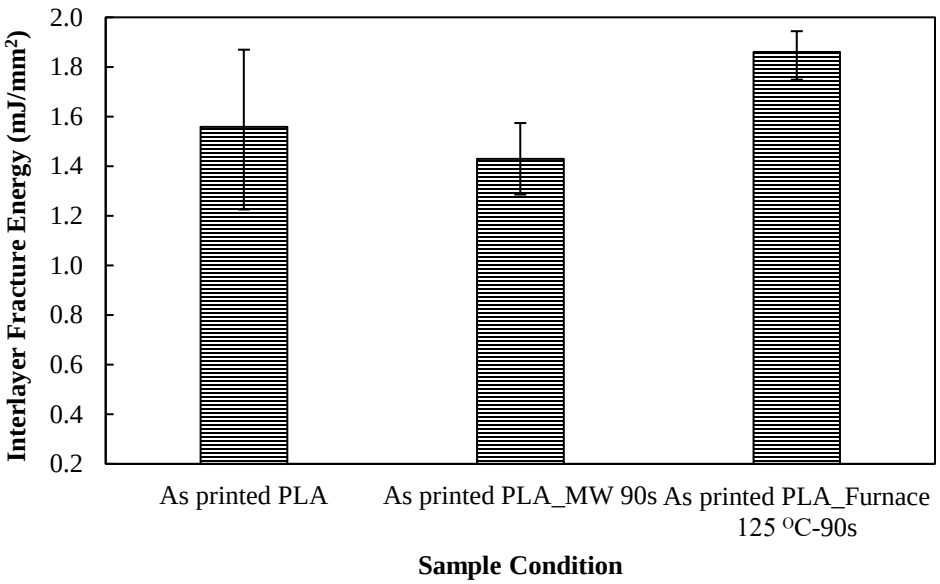

Fig. 30. Comparison of interlayer fracture energy values for as-printed and treated PLA samples.

Further studies are required to verify these speculations. The decrease in the degree of crystallinity can be the case for MW-treated samples under 90 seconds of exposure. The tensile test results show that beneficial or detrimental effects of process and material parameters during microwave exposure time on fracture energy have been neutralized.

CHAPTER IV

CONCLUSION AND FUTURE WORK

4.1 Conclusion

The ability to directly use different particulate fillers with the matrix filament during composite additive manufacturing provides the opportunity for customization of inhomogeneities and their distribution in the structure of products. It will also reduce the processing steps and time.

In this study, a manufacturing process was developed to customize the amount and distribution of copper filler in the layered structure of a PLA matrix. The principal findings of this study are summarized as follows:

a) The mass measurement analysis showed that the increase in depth of the grooves (that were made by the knurling of PLA filament) increased the mass of powders in the grooves. Also, the starch helped compact the powder particles and improved the packing density inside of grooves prior to additive manufacturing. In general, the spherical powders showed a higher packing density than the dendritic powders.

b) The analysis of the tensile test results indicated the decrease in fracture energy for the composites due to the presence of coppers compared with the PLA. The lower strength of composite samples was attributed to the higher area percentage of imperfections in the interlayer regions. The as-printed non-starched Cu/PLA composite samples showed higher fracture energy than the as-printed starched Cu/PLA samples. This result pointed out the adverse effect of increased copper percentage on the fracture energy of additively manufactured products.

c) The fractography analysis revealed some large eye ball shaped voids at the fracture surface of as printed PLA samples. In contrast, the voids were smaller and higher in area percentage for the composites. The observation suggested that the copper particles helped in the nucleation of voids at the interface between copper particles and PLA matrix.

d) It was hypothesized that the voids reduced the contact area and increased the residual stress inside the printed structure and at the interlayer areas of manufactured samples.

e) The microwave exposure for 75 seconds increased the fracture energy of the starched composite samples in comparison with the as-printed ones. The increase in the fracture energy was attributed to the interaction of copper particles with microwaves during heat treatment.

4.2 Future Work

As a newly proposed manufacturing model, the idea introduced in this study opens up many new doors for future works. The opportunities in the additive manufacturing industry are tremendous, and a small step was taken during this study for the advancement of this technology. The future works for further development of this proposed idea can be focused on the following aspects:

a) A computational model can be developed to understand the flow behavior during the deposition and effect of temperature at the printing stage. It would help analyze the flow

mechanism during deposition and modify the process parameters accordingly for improving the functional properties of the product.

b) Some experimental tests, such as thermogravimetric analysis (TGA), can be conducted for experimentally measuring the actual amount of filler after the printing process.

c) The study of the degree of crystallinity at the interface between copper particles and the PLA matrix through thermal analysis, such as the analysis by DSC tests, would help better understand the fracture behavior of the as printed and heat-treated composites.

d) Higher precision in controlling the amount of filler and porosity in the impregnation stage can be the subject of studies for further development of the PMC additive manufacturing process.

REFERENCES

1. Gupta, Nikhil, and Mrityunjay Doddamani. "Polymer Matrix Composites" JOM 70, no. 7 (2018): 1282-1283.

2. Kessler, Michael R. "Polymer matrix composites: A perspective for a special issue of polymer reviews" Polymer Reviews 52, no. 3 (2012): 229-233.

3. David A. Jesson & John F. Watts "The Interface and Interphase in Polymer Matrix Composites: Effect on Mechanical Properties and Methods for Identification" Polymer Reviews (2012), 52:3, 321-354.

4. Ru-Min Wang, Shui-Rong Zheng, Ya-Ping Zheng "Introduction to polymer matrix composites" Woodhead Publishing, 2011, Pages 1-548, ISBN 9780857092212.

5. Strong, A. Brent. "Fundamentals of composites manufacturing: materials, methods and applications" Society of Manufacturing Engineers, 2008.

6. Spanoudakis, J., and R. J. Young. "Crack propagation in a glass particle-filled epoxy resin" Journal of Materials Science 19, no. 2 (1984): 473-486.

7. Spanoudakis, J., R.J. Young "Crack-propagation in a glass particle-filled epoxy-resin. 2. Effect of particle matrix adhesion" Journal of Materials Science1984, 19, 487–496.

8. Sqcarl zwehen, General Electric Co. "Assessment of the Science Base for Composite Materials" A contractor report prepared for OTA, December 1985.

9. Varga, Cs, N. Miskolczi, L. Bartha, and G. Lipóczi. "Improving the mechanical properties of glass-fibre-reinforced polyester composites by modification of fibre surface" Materials & Design 31, no. 1 (2010): 185-193.

10. Jiao, Weizhou, Youzhi Liu, and Guisheng Qi. "Studies on mechanical properties of epoxy composites filled with the grafted particles PGMA/Al2O3" Composites Science and Technology 69, no. 3-4 (2009): 391-395.

11. Varga, Cs, N. Miskolczi, L. Bartha, and G. Lipóczi. "Improving the mechanical properties of glass-fibre-reinforced polyester composites by modification of fibre surface" Materials & Design 31, no. 1 (2010): 185-193.

12. Campbell, Flake C. "Structural composite materials" ASM international, 2010.

13. Yasmin, Asma, and Isaac M. Daniel. "Mechanical and thermal properties of graphite platelet/epoxy composites" Polymer 45, no. 24 (2004): 8211-8219.

14. Reginald B. Stoops, R.B. Stoops& Associates, Newport, R, "Manufacturing Requirements of Polymer Matrix Composites" Contractor report for OTA, December 1985.

15. According to information supplied by the USDA'S Office of Critical Materials.

16. Grimshaw, Michael N., Carroll G. Grant, and Jose Manuel Luna Diaz. "Advanced technology tape laying for affordable manufacturing of large composite structures" In International sampe symposium and exhibition, pp. 2484-2494. SAMPE; 1999, 2001.

17. Goh, Guo Dong, Yee Ling Yap, H. K. J. Tan, Swee Leong Sing, Guo Liang Goh, and Wai Yee Yeong. "Process–structure–properties in polymer additive manufacturing via material extrusion: A review." Critical Reviews in Solid State and Materials Sciences 45, no. 2 (2020): 113-133.

18. Mazumder, S.K. (ed.). (2002). "Composites Manufacturing, Materials, Product and Process Engineering" CRC Taylor & Francis, ISBN 0-8493-0585-3.

19. Gibson, Ian, David W. Rosen, and Brent Stucker. "Additive manufacturing technologies" Vol. 17. New York: Springer, 2014.

20. Booth, Joran W., Jeffrey Alperovich, Pratik Chawla, Jiayan Ma, Tahira N. Reid, and Karthik Ramani. "The design for additive manufacturing worksheet" Journal of Mechanical Design 139, no. 10 (2017).

21. Weber, Christopher, Vanessa Peña, Maxwell Micali, Elmer Yglesias, Sally Rood, Justin A. Scott, and Bhavya Lal. "The role of the national science foundation in the origin and evolution of additive manufacturing in the United States" Science & Technology Policy Institute 1 (2013).

22. Kochan, Anna. "Features Rapid growth for rapid prototyping" Assembly Automation (1997).

23. Wohlers TT. Wohler's report 2015 "Additive manufacturing and 3D printing state of the industry" Annual worldwide progress report, 2015.

24. R. Noorani "Rapid Prototyping—Principles and Applications" John Wiley & Sons, 2006.

25. Grimm, Todd. "User's guide to rapid prototyping" Society of Manufacturing Engineers, 2004.

26. Prakash, K. Satish, T. Nancharaih, and VV Subba Rao. "Additive manufacturing techniques in manufacturing-an overview" Materials Today: Proceedings 5, no. 2 (2018): 3873-3882.

27. Kruth, Jean-Pierre, Ming-Chuan Leu, and Terunaga Nakagawa. "Progress in additive manufacturing and rapid prototyping" CIRP Annals-Manufacturing Technology 47, no. 2 (1998): 525-540.

28. Gu, Hongbo, Chao Ma, Junwei Gu, Jiang Guo, Xingru Yan, Jiangnan Huang, Qiuyu Zhang, and Zhanhu Guo. "An overview of multifunctional epoxy nanocomposites" Journal of Materials Chemistry C 4, no. 25 (2016): 5890-5906.

29. Huang, Samuel H., Peng Liu, Abhiram Mokasdar, and Liang Hou. "Additive manufacturing and its societal impact: a literature review" The International Journal of Advanced Manufacturing Technology 67, no. 5-8 (2013): 1191-1203.

30. Wang, Xin, Man Jiang, Zuowan Zhou, Jihua Gou, and David Hui. "3D printing of polymer matrix composites: A review and prospective" Composites Part B: Engineering 110 (2017): 442-458.

31. Van Der Klift, Frank, Yoichiro Koga, Akira Todoroki, Masahito Ueda, Yoshiyasu Hirano, and Ryosuke Matsuzaki. "3D printing of continuous carbon fibre reinforced thermo-plastic (CFRTP) tensile test specimens" Open Journal of Composite Materials 6, no. 01 (2016): 18.

32. Tian, Xiaoyong, Tengfei Liu, Chuncheng Yang, Qingrui Wang, and Dichen Li. "Interface and performance of 3D printed continuous carbon fiber reinforced PLA composites" Composites Part A: Applied Science and Manufacturing 88 (2016): 198-205.

33. Matsuzaki, Ryosuke, Masahito Ueda, Masaki Namiki, Tae-Kun Jeong, Hirosuke Asahara, Keisuke Horiguchi, Taishi Nakamura, Akira Todoroki, and Yoshiyasu Hirano. "Three-dimensional printing of continuous-fiber composites by in-nozzle impregnation" Scientific reports 6 (2016): 23058.

34. Namiki, Masaki, Masahito Ueda, Akira Todoroki, Yoshiyasu Hirano, and Ryosuke Matsuzaki. "3D printing of continuous fiber reinforced plastic" In SAMPE Tech Seattle 2014 Conference. Soc. for the Advancement of Material and Process Engineering, 2014.

35. Zhong, Weihong, Fan Li, Zuoguang Zhang, Lulu Song, and Zhimin Li. "Research on rapid-prototyping/part manufacturing (RP&M) for the continuous fiber reinforced composite" Materials and Manufacturing Processes 16, no. 1 (2001): 17-26.

36. Nakagawa, Yuki, Ken-ichiro Mori, and Tomoyoshi Maeno. "3D printing of carbon fibre-reinforced plastic parts" The International Journal of Advanced Manufacturing Technology 91, no. 5-8 (2017): 2811-2817.

37. Guo, Nannan, and Ming C. Leu. "Additive manufacturing: technology, applications and research needs" Frontiers of Mechanical Engineering 8, no. 3 (2013): 215-243.

38. Zhong, Weihong, Fan Li, Zuoguang Zhang, Lulu Song, and Zhimin Li. "Short fiber reinforced composites for fused deposition modeling" Materials Science and Engineering: A 301, no. 2 (2001): 125-130.

39. Carneiro, Olga S., A. F. Silva, and Rui Gomes. "Fused deposition modeling with polypropylene" Materials & Design 83 (2015): 768-776.

40. Tekinalp, Halil L., Vlastimil Kunc, Gregorio M. Velez-Garcia, Chad E. Duty, Lonnie J. Love, Amit K. Naskar, Craig A. Blue, and Soydan Ozcan. "Highly oriented carbon fiber–polymer composites via additive manufacturing" Composites Science and Technology 105 (2014): 144-150.

41. Wang, Jianlei, Hongmei Xie, Zixiang Weng, T. Senthil, and Lixin Wu. "A novel approach to improve mechanical properties of parts fabricated by fused deposition modeling" Materials & Design 105 (2016): 152-159.

42. Shofner, M. L., Francisco Javier Rodríguez-Macías, Ranji Vaidyanathan, and Enrique V. Barrera. "Single wall nanotube and vapor grown carbon fiber reinforced polymers processed by extrusion freeform fabrication" Composites Part A: Applied Science and Manufacturing 34, no. 12 (2003): 1207-1217.

43. Le Duigou, A., M. Castro, R. Bevan, and N. Martin. "3D printing of wood fibre biocomposites: From mechanical to actuation functionality" Materials & Design 96 (2016): 106-114.

44. Ning, Fuda, Weilong Cong, Jingjing Qiu, Junhua Wei, and Shiren Wang. "Additive manufacturing of carbon fiber reinforced thermoplastic composites using fused deposition modeling" Composites Part B: Engineering 80 (2015): 369-378.

45. Compton, Brett G., and Jennifer A. Lewis. "3D-printing of lightweight cellular composites" Advanced materials 26, no. 34 (2014): 5930-5935.

46. Goodridge, Ruth Davina, Meisha L. Shofner, Richard JM Hague, Michael McClelland, M. R. Schlea, R. B. Johnson, and Christopher J. Tuck. "Processing of a Polyamide-12/carbon nanofibre composite by laser sintering" Polymer Testing 30, no. 1 (2011): 94-100.

47. Nikzad, Mostafa, S. H. Masood, and Igor Sbarski. "Thermo-mechanical properties of a highly filled polymeric composites for fused deposition modeling" Materials & Design 32, no. 6 (2011): 3448-3456.

48. Boparai, Kamaljit, Rupinder Singh, and Harwinder Singh. "Comparison of tribological behaviour for Nylon6-Al-Al2O3 and ABS parts fabricated by fused deposition modelling: This paper reports a low cost composite material that is more wear-resistant than conventional ABS" Virtual and Physical Prototyping 10, no. 2 (2015): 59-66.

49. Shemelya, Corey M., Armando Rivera, Angel Torrado Perez, Carmen Rocha, M. I. N. Liang, Xiaoju Yu, Craig Kief et al. "Mechanical, electromagnetic, and X-ray shielding characterization of a 3D printable tungsten–polycarbonate polymer matrix composite for space-based applications" Journal of Electronic Materials 44, no. 8 (2015): 2598-2607.

50. Ayrilmis, Nadir, Mirko Kariz, Jin Heon Kwon, and Manja Kitek Kuzman. "Effect of printing layer thickness on water absorption and mechanical properties of 3D-printed wood/PLA composite materials" The International Journal of Advanced Manufacturing Technology 102, no. 5-8 (2019): 2195-2200.

51. Hwang, Seyeon, Edgar I. Reyes, Kyoung-sik Moon, Raymond C. Rumpf, and Nam Soo Kim. "Thermo-mechanical characterization of metal/polymer composite filaments and printing parameter study for fused deposition modeling in the 3D printing process" Journal of Electronic Materials 44, no. 3 (2015): 771-777.

52. Castles, Flynn, Dmitry Isakov, A. Lui, Q. Lei, C. E. J. Dancer, Y. Wang, J. M. Janurudin, S. C. Speller, C. R. M. Grovenor, and Patrick S. Grant. "Microwave dielectric characterisation of 3D-printed BaTiO 3/ABS polymer composites" Scientific reports 6 (2016): 22714.

53. Chung D "Materials for thermal conduction" Applied Thermal Engineering 21(16) (2001):1593–1605.

54. Perez, Angel R. Torrado, David A. Roberson, and Ryan B. Wicker. "Fracture surface analysis of 3D-printed tensile specimens of novel ABS-based materials" Journal of Failure Analysis and Prevention 14, no. 3 (2014): 343-353.

55. Kokkinis, Dimitri, Manuel Schaffner, and André R. Studart. "Multimaterial magnetically assisted 3D printing of composite materials" Nature communications 6, no. 1 (2015): 1-10.

56. Martin, Joshua J., Brad E. Fiore, and Randall M. Erb. "Designing bioinspired composite reinforcement architectures via 3D magnetic printing" Nature communications 6, no. 1 (2015): 1-7.

57. Kalsoom, U., A. Peristyy, P. N. Nesterenko, and B. Paull. "A 3D printable diamond polymer composite: a novel material for fabrication of low cost thermally conducting devices" RSC advances 6, no. 44 (2016): 38140-38147.

58. Kurimoto, Muneaki, Yuu Yamashita, Hiroya Ozaki, Takeyoshi Kato, Toshihisa Funabashi, and Yasuo Suzuoki. "3D printing of conical insulating spacer using alumina/UV-cured-resin composite" In 2015 IEEE Conference on Electrical Insulation and Dielectric Phenomena (CEIDP), pp. 463-466. IEEE, 2015.

59. Boyle, Bret M., Panupoan T. Xiong, Tara E. Mensch, Timothy J. Werder, and Garret M. Miyake. "3D printing using powder melt extrusion" Additive Manufacturing 29 (2019): 100811.

60. Basher, Samiul, Kumkum Ahmed, Azusa Saito, Ajit Khosla, Masaru Kawakami, and Hidemitsu Furukawa. "Development of multi-material 3D printer" In Nano-, Bio-, Info-Tech Sensors, and 3D Systems II, vol. 10597, p. 105970K. International Society for Optics and Photonics, 2018.

61. https://www.makerbot.com/3d-printers/materials/method-pla/. Accessed 11 July 2020.

62. Chacón, J. M., Miguel Angel Caminero, Eustaquio García-Plaza, and Pedro J. Núnez. "Additive manufacturing of PLA structures using fused deposition modelling: Effect of process parameters on mechanical properties and their optimal selection" Materials & Design 124 (2017): 143-157.

63. Popescu, Diana, Aurelian Zapciu, Catalin Amza, Florin Baciu, and Rodica Marinescu. "FDM process parameters influence over the mechanical properties of polymer specimens: A review" Polymer Testing 69 (2018): 157-166.

64. Mullin, J. "Microwave processing" In New methods of food preservation, pp. 112-134. Springer, Boston, MA, 1995.

65. Thostenson, E. T., and T-W. Chou. "Microwave processing: fundamentals and applications" Composites Part A: Applied Science and Manufacturing 30, no. 9 (1999): 1055-1071.

66. Ulloa, Rafael Zamorano, Ma Guadalupe Hernandez Santiago, and Veronica L. Villegas Rueda. "The Interaction of Microwaves with Materials of Different Properties" In Electromagnetic Fields and Waves. IntechOpen, 2019.

67. Metaxas, AC and, and Roger J. “Meredith. Industrial microwave heating” No. 4. IET, 1983.

68. Mishra, Radha Raman, and Apurbba Kumar Sharma. "Microwave–material interaction phenomena: heating mechanisms, challenges and opportunities in material processing" Composites Part A: Applied Science and Manufacturing 81 (2016): 78-97.

69. Yarlagadda, Prasad KDV, and Tan Chuan Chai. "An investigation into welding of engineering thermoplastics using focused microwave energy" Journal of Materials Processing Technology 74, no. 1-3 (1998): 199-212.

70. Ku, Harry S., Fred Siu, Elias Siores, and James AR Ball. "Variable frequency microwave (VFM) processing facilities and application in processing thermoplastic matrix composites" Journal of materials processing technology 139, no. 1-3 (2003): 291-295.

71. Ku, H. S., F. Siu, E. Siores, J. A. R. Ball, and A. S. Blicblau. "Applications of fixed and variable frequency microwave (VFM) facilities in polymeric materials processing and joining" Journal of Materials Processing Technology 113, no. 1-3 (2001): 184-188.

72. Singh, Inderdeep, Pramendra Kumar Bajpai, Deepak Malik, Apurbba Kumar Sharma, and Pradeep Kumar. "Feasibility Study on Microwave Joining of 'green composites'" Akademeia 1, no. 1 (2011): ea0101.

73. Sweeney, Charles B., Blake A. Lackey, Martin J. Pospisil, Thomas C. Achee, Victoria K. Hicks, Aaron G. Moran, Blake R. Teipel, Mohammad A. Saed, and Micah J. Green. "Welding of 3D-printed carbon nanotube–polymer composites by locally induced microwave heating" Science advances 3, no. 6 (2017): e1700262.

74. Wang, Yanqing, Zengguang Liu, Huwei Gu, Chunzhi Cui, and Jingbin Hao. "Improved mechanical properties of 3D-printed SiC/PLA composite parts by microwave heating" Journal of Materials Research 34, no. 20 (2019): 3412-3419.

75. Jacob, J., L. H. L. Chia, and F. Y. C. Boey. "Thermal and non-thermal interaction of microwave radiation with materials" Journal of materials science 30, no. 21 (1995): 5321-5327.

76. Rybakov, K. I., V. E. Semenov, S. V. Egorov, A. G. Eremeev, I. V. Plotnikov, and Yu V. Bykov. "Microwave heating of conductive powder materials" Journal of Applied Physics 99, no. 2 (2006): 023506.

77. Yamada, Shuji, Jinko Kanno, and Miki Miyauchi. "Multi-sized sphere packing in containers: optimization formula for obtaining the highest density with two different sized spheres" Information and Media Technologies 6, no. 2 (2011): 493-500.

78. Noori, Hadi. "Interlayer fracture energy of 3D-printed PLA material" The International Journal of Advanced Manufacturing Technology 101, no. 5-8 (2019): 1959-1965.

VITA

Nazmul Haque

Candidate for the Degree of

Master of Science

Thesis: IN-SITU IMPREGNATION OF POLYMER MATRIX WITH COPPER POWDER DURING ADDITIVE MANUFACTURING

Major Field: Mechanical and Aerospace Engineering

Biographical:

Education:

Completed the requirements for the Master of Science in Mechanical and Aerospace Engineering at Oklahoma State University, Stillwater, Oklahoma in July, 2020.

Completed the requirements for the Bachelor of Science in Naval Architecture and Marine Engineering at Bangladesh University of Engineering & Technology, Dhaka, Bangladesh in 2017.